Trait-based paleontological niche prediction recovers extinct ecological breadth of the earliest specialized ant predators

Christine Sosiak, Tyler Janovitz, Vincent Perrichot, John Paul Timonera, Phillip Barden

Trait-based paleontological niche prediction recovers extinct ecological breadth of the earliest specialized ant predators

Authors: Christine Sosiak,*[1] Tyler Janovitz,[2] Vincent Perrichot,[3] John Paul Timonera,[4] Phillip Barden[1,5]

Affiliations: 1. Federated Department of Biological Sciences, New Jersey Institute of Technology; 2. Foundation Medicine Inc.; 3. Géosciences Rennes, Université de Rennes, CNRS; 4. Biological Sciences Program, St. Mary's University; 5. Division of Invertebrate Zoology, American Museum of Natural History

***Corresponding author:** Christine Sosiak, ces43@njit.edu

ORCIDs: Christine Sosiak: 0000-0002-9057-8636; Phillip Barden: 0000-0001-6277-320X

Keywords: paleoecology; ants; morphology; machine learning

MS type: E-article

Abstract

Paleoecological estimation is fundamental to the reconstruction of evolutionary and environmental histories. The ant fossil record preserves a range of species in three-dimensional fidelity and chronicles faunal turnover across the Cretaceous and Cenozoic; taxonomically rich and ecologically diverse, ants are an exemplar system to test new methods of paleoecological estimation in evaluating hypotheses. We apply a broad extant ecomorphological dataset to evaluate Random Forest machine learning classification in predicting the total ecological breadth of extinct and enigmatic “hell ants”. In contrast to previous hypotheses of extinction-prone arboreality, we find hell ants were primarily leaf litter or ground-nesting and foraging predators, and by comparing ecospace occupations of hell ants and their extant analogues, we recover a signature of ecomorphological turnover across temporally and phylogenetically distinct lineages on opposing sides of the KPg boundary. This paleoecological predictive framework is applicable across lineages and may provide new avenues for testing hypotheses over deep time.

Introduction

Estimating the ecological niche occupation of extinct taxa is a central component of paleontology. The putative ecologies of extinct organisms are routinely incorporated into analyses of extinction risk, paleoenvironmental reconstruction, and lineage evolutionary history (Palmqvist et al. 2003; Benson et al. 2014; Frederickson et al. 2018). Even as aspects of extinct species' niche occupation may be reliably inferred by the preservation of individual traits in fossil specimens, organismal ecology remains multifaceted. Morphology may often - though not always (Miller et al. 2017) - reflect ecology across entire phenotypes (Williams 1972; Losos 1992) and phenotypes may be linked to multiple aspects of an organism's ecological niche spanning habitat, diet, and interactions. These ecologically-linked body plans – ecomorphs – are found in such disparate taxa as fish, reptiles, arthropods, and mammals (Barton et al. 2011; Gerry et al. 2011; Sanders et al. 2013; Figueirido et al. 2019). The relationship between ecological niche and multi-trait morphology can also be leveraged to estimate paleoecologies. In lineages with surviving relatives, extant taxa may serve as data-rich analogs for ecological niche estimation: however, the partial preservation of many fossil specimens and aberrant phenotypes in some extinct lineages may reduce the utility of extant-to-extinct comparisons.

Across vertebrate species, limb anatomy is a predictor of locomotion, prey items, and substrate behaviour. In particular, the forelimb anatomy of carnivores has been used to predict the likely predatory habits and prey size of extinct carnivorous mammals and mammaliaforms (Dunn et al. 2019; Ercoli et al. 2012; Figueirido et al. 2016; Jenkins et al. 2020; Lungmus and Angielczyk 2021; Meloro and Louys 2014). Other examples of the morphology of extant species being used in the prediction of extinct species' ecology include estimating diet in extinct raptor species from present-day birds of prey (Hertel 1995); predicting prey items and modes of scavenging in extinct crocodyliforms from extant crocodyliform snout morphology (Drumheller and Wilberg 2019); approximating arboreal behaviour in extinct primates (Rector and Vergamini 2018); and predicting habitat preferences in fossil *Anolis* lizards using ear canal shape (Dickson

et al. 2017). In many cases, these methods incorporate isolated body parts rather than full-body morphology, potentially because trait ecomorphology has been more intensely studied in vertebrates than in other animal taxa, and is thus more well-defined. However, morphometric analyses of full mammalian skeletons have been used to predict the locomotion mode of various Mesozoic mammaliaforms (Chen and Wilson 2015; Meng et al. 2017).

Attempts to predict paleoecology from extant morphology frequently use techniques such as canonical correlations analysis or canonical variate analysis, and in particular linear discriminant analysis (Dickson et al. 2017; Dunn et al. 2019; Hertel 1995; Janis and Figueirido 2014; Meloro and Louys 2014; Rector and Vergamini 2018). These methods maximize variation in the measured traits between predetermined classes in morphospace. The fossil specimen's most likely ecology is then determined by proximity to each class mean in this constructed morphospace (Strauss 2010). These approaches are powerful tools for establishing sets of traits most strongly associated with predetermined classes, but are limited to linear relationships only among measured traits, which may restrict accuracy by failing to incorporate non-linear predictive relationships between traits.

While most predictive paleoecology studies have focused on vertebrate paleoecology, minimal attention has been paid to these approaches in invertebrates, particularly insects. Many extant insect lineages reach back to the Mesozoic or Paleozoic, and are highly ecologically diverse. One example are the ants, which arose between ~150 and 100 Ma (Mega-annum) (Moreau et al. 2006; Brady et al. 2006; Borowiec et al. 2019). With over 15,000 species comprising a significant component of terrestrial biomass, ants are globally ubiquitous, speciose, and are present in most post-producer ecological niches (Hölldobler and Wilson 1990; Bolton 2021). Importantly, despite this ecological diversity, ants are also morphologically conserved with respect to broad body plan functionality and possess a rich fossil record extending 100 Ma to the mid-Cretaceous. A majority of ant fossils are known from fossil amber, which often preserves entire specimens with high fidelity. Because of their well-defined

homology and uniquely preserved fossil history, extinct ants are strongly suited for testing paleoecological niche prediction methods.

The earliest known ant fossils date to the Early–Late Cretaceous transition and comprise extinct stem lineages that began to diversify prior to the most recent common ancestor of all living ants. While crown lineages diversified concomitant with these stem lineages, all stem lineages went extinct near the end of the Cretaceous, while crown lineages persisted into the Cenozoic, exemplifying a distinct faunal turnover across the Cretaceous-Paleogene (KPg) boundary. Cretaceous fossils have fueled speculation on the ecological occupation of the earliest ants because these taxa have bearing on the evolution of eusociality more broadly. Early speculation on Cretaceous ant ecology posited that these early species were unlikely to construct nests, but instead used already-present cavities in soil and wood, based on assumptions that these early species were primitively eusocial and thus unlikely to cooperate as well in nest building, or that their mandible morphology was prohibitively specialized to allow for nest construction (Dlussky 1996; Wilson 1967; Wilson 1987a; Wilson 1987b; Grimaldi and Agosti 2000; Engel and Grimaldi 2005). Based on their presumed wasp ancestors, they were additionally argued to be predators (Dlussky 1996; Wilson 1987a; Wilson 1987b). As the taxonomic diversity of extinct ant species increased with the discovery of new fossils, paleoclimate and phylogenetic reconstructions suggested that early ants occupied soil and leaf litter microhabitats in newly emerging angiosperm forests (Wilson and Hölldobler 2005, Perrichot et al. 2008, Moreau et al. 2006, Moreau and Bell 2013). Phylogenetic reconstructions using extant lineages have also recovered ant ancestors as potentially hypogaeic soil-dwellers (Lucky et al. 2013). While there have been secondary inferences regarding the ecology of the earliest ants, no fossil-derived data have yet been included in the reconstruction of ancient ant ecology.

Haidomyrmecines, or hell ants, are an enigmatic and morphologically aberrant extinct subfamily of ants comprising 16 described species and 10 genera (Perrichot et al. 2020). Hell

ants occupy a stem group position relative to modern ants and are frequently recovered as sister to all other extinct and extant ants (Barden et al. 2016; 2020). They persisted throughout the mid-to-late Cretaceous as evidenced by amber fossils ranging from 100 to 78 Ma on three different continents in Canada, Myanmar, and France (Dlussky 1996; Perrichot et al. 2008; McKellar et al. 2013) and are hypothesized to have undergone extinction concomitant with the early radiation and diversification of extant lineages. These ants are morphologically unusual in having vertically-articulating mandibles, unlike the horizontal alignment of modern ants. Remarkably, hell ants possess an array of horn-like cranial appendages that have been directly observed to facilitate solitary predation through fossil remains (Barden et al. 2020): haidomyrmecines captured prey individually by articulating their mandibles against their horns. Hell ants have been hypothesized as arboreal predators, considering the potential difficulty of substrate manipulation with their vertically-aligned mandibles, and frequent preservation in amber, potentially indicating close proximity to tree resin (Dlussky 1996; Barden and Grimaldi 2012; Lattke and Melo 2020). Arboreality may be a risk factor in cataclysmic mass extinction events, given the dependency on habitats that are more exposed to extreme weather fluctuations and other extreme events such as wildfires, etc. (Field et al. 2018). If hell ants were indeed arboreal, it may have been a contributing factor to their extinction towards the end of the Cretaceous.

Were hell ants indeed arboreal, potentially increasing their risk of extinction? How do the ecologies of the earliest ants compare to extant lineages today? Did functional or ecological succession accompany ant faunal turnover from the Cretaceous to the Cenozoic? Here, we use a wide-ranging extant morphometric dataset spanning over 160 species that has previously demonstrated a quantitative link between morphology and ecology to predict the paleoecology of several hell ant species. Using a supervised machine learning classification algorithm, Random Forest, we predict foraging niche, nesting niche, and functional role for hell ants. With these predictions, we reconstruct known ecomorphological space for haidomyrmecines and

compare these ecological occupations to those of extant lineages of specialized solitary predators. Our results demonstrate repeated filling of functional niche space across phylogenetically and temporally distant lineages. This approach provides a generalizable framework for paleoecological estimation beyond either single-trait interpretations or subjective interpretations from taxonomic expertise, opening future directions for the reconstruction of extinct communities and ecosystems.

Methods

Extant morphological data sampling and ecological niche binnings

We sampled extant ant morphological data following the protocol of Sosiak and Barden (2021) (Figure 1). Our extant dataset spans 15 subfamilies, 113 genera, and 167 species, sampling three specimens per species where possible, and measuring as many conspecifics as were present in museum collections otherwise. Polymorphic species are represented by the media caste, or caste representing a morphological "midpoint" between small and large workers, and species with specialized castes are represented by non-specialized "minor" workers. There is currently no evidence for specialized hell ant worker castes, and specialized worker castes are not a synapomorphy of crown ants, informing our choices of caste sampling.

Our morphometric sampling comprised linear measurements of 12 cephalic traits and five post-cephalic traits (Table 1). Most sampled traits have been previously linked to ecology (Weiser and Kaspari 2006; Yates and Andrew 2011; Gibb et al. 2015; Yates et al. 2014). All measurements were conducted on point-mounted specimens under stereo microscopy. Because linear measurements alone may not fully capture important trait variation, and body size in diverse species can drive most variation in a dataset and potentially mask other important contributors, we created three datasets: one comprising raw linear measurements; one comprising shape ratios calculated from the linear measurements; and one size-corrected

dataset comprising log-shape variables and log-body length or Weber's length (Mosimann 1970). A list of all shape ratio traits with associated definitions may be found in Table S1.

All specimens were assigned a binning from each of three ecological niche aspect categories, following the protocol of Sosiak and Barden (2021): functional role (referring to the diet of the species), nesting niche (the type of nest and stratum in the environment), and foraging niche (the stratum in the environment where the species forages for food) (Figure 1, Table 2). Specimen binnings were assigned based on literature surveys. When any particular aspect of a species' ecological niche was uncertain, the species was assigned an "unknown" binning and excluded from further model training. We found 35 total observed combinations of niche binnings across all niche aspects and specimens; we additionally collapsed these 35 combinations into 10 simplified ecomorph syndromes (based on ecological and morphological overlap) to evaluate whole-body ecomorphological correlates. A list of all ecological niche aspect combinations and ecomorph syndromes with associated definitions may be found in Table S2.

Fossil morphological data sampling

We measured fossil hell ant specimens using a combination of stereo microscopy and reconstructions of X-ray micro-computed tomography (micro-CT) scans (Figure 1). All hell ant specimens were from Kachin amber (99 Ma). Twenty specimens from 16 species and morphospecies were measured under stereo microscopy. We submerged the amber specimens in water to reduce light distortion; some measurements were not possible due to specimen positioning. Three specimens were micro-CT scanned and reconstructed for subsequent measurements: two species of hell ant (*Haidomyrmex scimitarus* and *Linguamyrmex vladi*) and a *Pseudomyrmex macrops* specimen from Dominican amber (16 Ma) to assess the reliability of CT-scan based data. Congeners of the Dominican *Pseudomyrmex* fossil are extant today and their ecology is consistent across the genus and well-characterized. The *H. scimitarus*

(specimen AMNH Bu-FB80) and *L. vladi* (specimen AMNH BuPH-1) specimens were scanned at the American Museum of Natural History Microscopy and Imaging Facility using a GE phoenix v|tome|x s240 60kV CT-scanner. Specimen AMNH Bu-FB80 was imaged at 180 µA for 5 second exposures and a voxel size of ~8µm; specimen AMNH BuPH-1 at 250 µA for 1 second exposures and a voxel size of ~3µm. The *Pseudomyrmex macrops* specimen (AMNH DR-14-1021) was imaged at the New Jersey Institute of Technology York Center using a Bruker SkyScan 1275 at 60kV and 150µA for 1 second exposures with a subsequent voxel size of ~3.5µm. Volume reconstruction of the x-ray images was conducted in 3D Slicer v4.11 (Fedorov et al. 2012) using the Segmentation modules; still images of the reconstructed specimens were subsequently imported into ImageJ (Abràmoff et al. 2004) for linear measurements to retain consistency with measurements taken under stereo microscopy. Post-cranial morphology of hell ants is similar to extant ant species, while cranial morphology is highly aberrant. To ensure that we were assessing morphological variation in terms of both homologous and functional morphology, we partitioned data according to homologous or functional measurements; a full discussion of homologous versus functional morphology may be found in the Supplementary Information.

Due to limitations measuring specimens directly from amber fossils, we produced two fossil morphometric datasets: one 'incomplete' dataset which excluded a subset of traits for all specimens; and one with all measurements included. The incomplete dataset lacked the frontal head length, head width, frontal mandible length, and pronotal width measurements. These measurements are often difficult to accurately capture because amber fossils are typically prepared to expose a clear lateral profile of any specimen, leaving the dorsal and frontal margins of the amber rounded and distorted. Twenty hell ant specimens were included in this incomplete dataset. The complete dataset comprised the proof-of-concept fossil *Pseudomyrmex macrops* specimen and three hell ant specimens: *Dhagnathos autokrator, H. scimitarus,* and *L. vladi.* While the majority of specimens included were workers, two of the specimens – the

complete *D. autokrator* and *H. scimitarus* – were represented by alate (winged) and dealate (wings shed) queens, respectively. We included queens for two reasons: one, hell ant queens are hypothesized to have actively foraged and hunted in early colony foundation, and so likely occupied a similar ecological niche to the workers of the species; and two, fossilized worker specimens are not known for many hell ant species and are entirely unknown for the genus *Dhagnathos*. While we have no comparison for *Dhagnathos* workers, we include a *H. scimitarus* worker in the incomplete morphometric dataset, allowing us to compare the accuracy of the model in predicting queen and worker ecology. A full list of all specimens included with information pertaining to their sampling methods and castes can be found in Table S3; all morphometric data for fossil specimens may be found in the Supplementary Data.

To ensure that morphological diversity for traits measured from fossil species are within the bounds of extant morphological diversity, we conducted principal component analyses (PCA) to compare morphospace occupation of hell ants relative to extant lineages. We conducted separate PCAs for all three measurement datasets. All PCAs were implemented in R packages “corrplot” (Wei et al. 2017) and “FactoMineR” (Lê et al. 2008).

Model training and testing

We implemented Random Forest analysis, a supervised machine learning algorithm, to delimit species into ecological niche binnings by morphology. Random Forest algorithms rely on an ensemble of decision trees with each tree providing a ‘vote’ for a majority consensus determining the predicted class (Breiman 2001). Each decision tree is built through iteratively sampling the training dataset with replacement, with each internal node or ‘split’ in the tree being selected from the variable contributing highest accuracy from a randomly subsampled set of predictor variables. As the trees are iteratively built, each tree provides a ‘vote’ on the most likely class for each sample in the training dataset; the algorithm then uses the vote consensus to predict class for each sample. The iterative sampling or bagging of the training dataset to

build the trees and the randomly selected subset of variables at each node ensure that the decision trees are uncorrelated and that the model is not overfitted to the training dataset. Throughout model construction for each tree, Random Forest algorithms iteratively sample two-thirds of the provided training dataset for training the model and one-third of the provided dataset for testing the model; error rate across these iterations is then averaged to provide out-of-bag (OOB) error rate for the model. This removal of testing data during bootstrapping eliminates the need for *a priori* separation of a testing and training dataset, incorporating all collected data. Model parameters include *ntree* (the number of trees in the ensemble model) and *mtry* (the number of variables randomly selected to be tested at each split).

While other supervised machine learning or dimension reduction techniques are more commonly used in morphology-based paleoecological prediction, Random Forest has recently been shown to outperform linear predictive approaches with respect to morphology (Pigot et al. 2020; Sosiak and Barden 2021), hence our use here. We trained our Random Forest models using our extant ant morphometric dataset with known ecological niche binnings (Figure 1). We constructed Random Forest models for the linear measurements, shape ratios, and log-shape variable datasets separately for each ecological niche aspect and overall ecomorph syndrome, allowing for granular classification of ecological niche and more synthesized classification. Model parameters were selected based on initial sensitivity tests: *mtry*=4 and *ntree*=5000. Random Forest analyses were implemented in the R package 'randomForest' (Liaw and Weiner 2018).

Model implementation with extinct specimens

We implemented different sets of Random Forest models; given the missing traits in our incomplete dataset, models needed to be trained once with the missing traits eliminated from the extant ant morphometrics training dataset, and once including all traits measured for the complete fossil dataset (Figure 1). For each dataset (complete or incomplete), we implemented

three models: using the linear measurements, shape ratios, and log-shape variables. Using these three models, we predicted ecological niche aspects of hell ants twice: once using functional morphology, and once using homologous morphology. Thus, each specimen's ecological niche was predicted six times (contingent on whether their measurement set was complete or incomplete): using linear measurements with functional morphology, linear measurements with homologous morphology, shape ratios with functional morphology, shape ratios with homologous morphology, log-shape variables with functional morphology, and log-shape variables with homologous morphology. We compiled all model votes into a heatmap of model predictions for each specimen with the R package 'ggplot2' (Wickham 2016) to better visualize the consensus among models for each predicted ecological niche aspect.

Comparative ecomorphological niche occupation

To assess the specificity and breadth of niche occupations in haidomyrmecines, we generated three-dimensional ecomorphological matrices comprising living and extinct predatory taxa. Our taxonomic sampling included five lineages: hell ants, and four distantly related extant groups with trap-jaw like morphology and behavior, wherein workers act as solitary hunters that capture prey, many doing so through rapid closure of specialized mandibles (Gronenberg and Ehmer 1996, Hölldobler & Wilson 1990). While the speed of prey capture is not known in hell ants, haidomyrmecines are united with some extant trap-jaw taxa by the presence of elongate setae (interpreted as trigger hairs) in the path of mandible closure and dramatic morphological adaptations related to predation (Dlussky 1996; Barden and Grimaldi 2012). Importantly, all species within our sampling are primarily solitary hunters (Larabee et al. 2014; Barden et al. 2020) in contrast to group raiding or collective prey capture that typify many other predatory ant lineages (Dornhaus and Powell 2010). Trap-jaw mechanisms have evolved at least ten times in living ants (Larabee et al. 2014; Booher et al. 2021); these origins are distributed among four monophyletic lineages. Extant trap-jaw predation has evolved once within each of the

subfamilies Ponerinae and Formicinae, thus our sampling included species within relevant genera: *Anochetus* + *Odontomachus* (Ponerinae) and *Myrmoteras* (Formicinae), respectively. There are at least eight trap-jaw origins within the subfamily Myrmicinae and seven of these have occurred within the genus *Strumigenys*. Our myrmicine sampling therefore included *Strumigenys* as well as the five "dacetine" trap-jaw genera: *Acanthognathus*, *Daceton*, *Epopostruma*, *Microdaceton*, and *Orectognathus*. Although it is not yet clear whether all dacetine trap-jaws are the product of a single origin, we grouped these taxa in analyses as they are more closely related to each other than any are to *Strumigenys* (Ward et al. 2015).

To estimate the total number of unique ecomorphological combinations for each specialized predatory lineage, we gathered niche occupation and size data for a total of 982 species, including 15 hell ant species with ecologies estimated under random forest. Our extant sampling represents a minimum of 50% species sampling for each genus. Each species was assigned one of three foraging and three nesting niche aspects according to our modeling results for haidomyrmecines or published natural history observations for extant taxa (Supplementary Data_Trap Jaw Ecomorphospace). Because observational data do not exist for all species, we applied published generalizations in some cases (e.g. *Strumigenys* are noted as almost always leaf litter nesting and foraging, thus we assumed this occupation by default except when otherwise noted in the literature). For the predicted hell ant ecomorphological combinations, considering that there were multiple predictions using different models that did not always converge on the same predicted class, we constructed two matrices: an expansive one incorporating all ecomorphological combinations predicted across all models, and a conservative second matrix incorporating only predictions using the linear measurements dataset with functional morphology. All niche occupation and size data may be found in the Supplementary Data.

To estimate body size, we gathered minimum and maximum Weber's length (a measurement of mesosoma length and traditional metric of ant size) measurements from

taxonomic descriptions and revisions. To include taxa without published morphometric data, we collected Weber's length measurements from publicly available images on AntWeb (AntWeb 2021) using ImageJ version 1.53 (Schneider et al. 2012). We discretized species sizes by delimiting Weber's length ranges for each species into at least one of twelve equal size binnings. Size binning ranges were defined as one half of the standard deviation of Weber's length measurements across all species. In cases where a species Weber's length range exceeded any one size binning, we assigned multiple size binnings for that species.

We generated three-dimensional ecological disparity values for each lineage following a modification of Chen et al. (2019). We assigned each ecological binning a numerical value from 1 to 3 based on inferred ecological proximity (nesting niche: leaf litter = 1, ground = 2, lignicolous = 3; foraging niche: leaf litter = 1, epigaeic = 2, arboreal = 3), while values for the third ecological dimension, body size, were continuous from 1 to 12. We included raw body size as size can act as a constraint on ecological role in the environment. To reduce the impact of species sampling bias between fossil and extant lineages, we calculated ecological disparity only among unique occupations, not between species. We created a matrix of unique niche occupations for each lineage and calculated intra-lineage ecological disparity values by summing the distances between niche aspects for all pairwise combinations of unique occupations using the equation. For example, the ecological disparity between unique occupation 1 (uo1) and unique occupation 2 (uo2) would be: $| \text{Nesting Niche}_{uo1} - \text{Nesting Niche}_{uo2} | + | \text{Foraging Niche}_{uo1} - \text{Foraging Niche}_{uo2} | + | \text{Body Size}_{uo1} - \text{Body Size}_{uo2} |$. We summarized mean and standard deviations for each lineage using 'ggplot2' (Wickham 2016). Visual representations of lineage specific ecomorphological occupations (ecospaces) were generated using the R package "rgl" (Adler et al. 2021) and redrawn in Adobe Illustrator.

Results

Model performance and prediction accuracy

Visualization of extant and extinct morphospace through principal component analysis illustrated that extinct morphospace fully overlaps with extant morphospace representing linear trait measurements and log-shape variable measurements, and mostly overlaps with extant morphospace representing shape ratio measurements (Figures S3-5). Although aspects of hell ant morphology are distinct, hell ant morphospace represented by measurements incorporated in our models is primarily within the bounds of extant diversity. Principal component 1 in the shape ratio morphospace is primarily driven by mandible size relative to body size, which is greater in many hell ants compared to extant ants, likely resulting in the small portion of unique hell ant morphospace. Predictions from shape ratio measurements are often not significantly different from predictions using linear measurements or log-shape variable measurements, however, and this along with a great degree of morphospace overlap suggests that extant morphology is an appropriate analog for extinct ecomorphology.

Out-of-bag error rate estimates ranged from 11-22%, reflecting accuracies of 78-89% depending on the training data partition used and the ecological niche aspect being predicted. While models trained on the linear measurement and log-shape variable measurement datasets were typically more accurate than the shape ratio dataset, this was not always the case, and the accuracies were not higher by more than a few percentage points. Consistently, nesting niche and foraging niche were predicted with higher accuracy, while functional role and ecomorph models generally had lower accuracy. Models trained on the complete morphometric dataset were more accurate compared to those trained on the subset morphometric dataset, though the difference was generally only a few percentage points. Additionally, model consensus votes were highest with foraging niche and nesting niche predictions, indicating overall greater confidence in the accuracy of these predictions; while functional role and ecomorph had lower consensus vote totals (Figure 2, Table 3, Tables S4-51). Trait importance to model accuracies

varied somewhat between models, but overall we found eyes, mandibles, legs, antennae, and body size to be essential to model accuracy (Figures S6-8).

The fossil *Pseudomyrmex macrops* specimen used as a proof-of-concept was consistently and accurately predicted as a lignicolous arboreal-foraging phytophagivore (Figure 2). The arboreal foraging niche was predicted with the highest confidence, while the phytophagous functional role was predicted with the lowest confidence (Figure 2, Tables S4-S27).

Hell ants are primarily recovered as epigaeic foragers that nested directly on the ground surface, though several species are predicted as leaf litter nesters and foragers (Figure 2). Additionally, one *Haidomyrmex* morphospecies (*H. sp3*) was partially predicted as a lignicolous nester and arboreal forager, with *Linguamyrmex brevicornis* also partially predicted as an arboreal forager. Hell ants were primarily predicted as predators, both specialist and generalist, though some species were additionally predicted to be omnivorous (Figure 2, Tables S4-51). Supporting the general accuracy of our models, we find broad congruence across species when multiple conspecifics were included, and also do not recover any strong predictions of unlikely ecological niches: hell ants were not predicted as subterranean nesters, column-raiding foragers, or fungivorous, granivorous, or phytophagous functional roles (Figure 2).

Specimen consensus among the six models used was variable. For some specimens, there was very strong agreement, with all six models predicting the same ecological niche aspect binning; however, there were also cases where two models predicted one niche aspect binning and two predicted another (Figure 2, Tables S4-51). There were rarely scenarios where more than two different niche aspect binnings were predicted for a single specimen. More frequently, in cases of split predictions, the shape ratio models or log-shape variable models would predict the same aspect binning while the linear measurement models would predict another, as opposed to scenarios where predictions would split along the lines of functional versus homologous morphology used in the testing dataset.

We found no robust differences in niche predictions between specimens measured directly and specimens measured from microCT reconstructions; specimens measured from microCT reconstructions were also predicted as epigaeic or leaf litter foragers and nesters (Figure 2, Tables S4-51). Additionally, we find that the dealate *Haidomyrmex scimitarus* (measured from a microCT reconstruction) and the worker *H. scimitarus* (measured using light microscopy) were both predicted to be ground-nesting epigaeic predators (Figure 2, Tables S4-51); illustrating consensus between the two types of input testing data.

Niche occupation in extinct and extant specialized predators

Our most conservative estimates of ecological niche occupation suggest that hell ants occupied primarily ground-nesting epigaeic niches with some leaf litter occupation, while across-model results recover hell ants within arboreal, ground, and leaf litter niches across a moderate body size range. In comparing predicted hell ant ecospace to solitary predator ant ecospace, we find that hell ants occupied at least part of the ecomorphological spaces occupied by each extant trap-jaw lineage (Figure 3). The sister ponerine genera *Anochetus* and *Odontomachus* exhibit the greatest extant ecospace diversity and ecological disparity, occupying most potential ecospace, with species ranging from ~3mm to ~1.7cm spanning arboreal, ground, and leaf litter niches (Brown 1978, Hoenle et al. 2020). The most restricted ecospace is occupied by species within the formicine genus *Myrmoteras*, which are minute leaf litter dwellers. The most taxonomically diverse trap-jaw lineage is *Strumigenys* with over 850 species, but the constrained size and primarily leaf litter habits of the genus produce a within-group ecological disparity that is low relative to the ponerine lineages with 188 total species (Bolton 2021). Similarly, while total species diversity of hell ants is unknown, even within our limited fossil sample, haidomyrmecines are found to be relatively ecologically disparate and diverse compared to extant lineages.

Discussion

We present here a pipeline for paleoecological niche estimation using machine learning and broad ecomorphological sampling. Because this class of supervised machine learning incorporates non-linear modeling and has been shown to outperform other discriminant function methods (Pigot et al. 2020; Sosiak and Barden 2021), it represents a powerful tool in the reconstruction of fossil niche occupations. Considerations identified through sensitivity analysis include alternative assumptions of input data, hypotheses of homology, and dataset completeness. Through implementation of this method, we find broad consensus across models for hell ants as leaf litter foraging-and-nesting or epigaeic ground-nesting predators, in contrast to previous assumptions regarding hell ant ecology. Paleoecological niche estimation reveals repeated ecological niche occupation across ant taxa, even across Earth's last major extinction boundary, suggesting functional succession in ant lineages through deep time.

Utility of Random Forest in paleoecological estimation

Our results demonstrate the utility of amber specimens in paleoecological estimation and the capacity for microCT reconstructions to aid in data collection. The congruence between the known ecology of extant *Pseudomyrmex* species and the predicted ecology of our sampled fossil *Pseudomyrmex macrops* specimen highlights both that taphonomic preservation of amber specimens does not prohibitively distort morphology, and that microCT data from fossil specimens is congruent with morphological data collection derived from extant taxa.

Estimates from our Random Forest models emphasize the need for selectivity and caution in assembling training data. We find that accuracy and congruence among our models was influenced more by the input training data, rather than the usage of either functional or homologous morphology in testing data: i.e., models trained on linear measurement data tended to predict the same nesting or foraging class for hell ants regardless of whether functional or homologous morphology was considered, while models trained on other datasets might predict

a different ecology. This trend may reflect variable importance; traits in hell ants that were measured differently based on alternate assumptions of homology were also traits that were not ranked as highly important to model accuracy, therefore homology assumptions may not have made much difference to the ultimate predicted class. However, this trend may not hold true in other taxa where a questionably homologous trait is of much greater importance to its ecological niche, such cases should be evaluated through assessments of trait importance in model construction. Additionally, we found only a minor loss in model accuracy from models trained on the complete morphometric dataset (17 traits) relative to models trained on the subset morphometric dataset (13 traits). Many of the measurements left out in the subset dataset were ranked as of low importance in the accuracy of the model, highlighting again the necessity of identifying important variables to model accuracy. While the problem of extraneous variables in the model itself is one mostly of unnecessary computing power, it is important to identify crucial traits when sampling fossil data to collate the greatest number of sufficiently complete specimens.

Sources of intraspecific and inter-specimen variability in Random Forest model predictions range from model error to actual ecological variability within the taxa sampled. While we found that each of the six models did not always predict the same ecological niche for one specimen, most frequently these differences were between niche aspects that were physically or ecologically proximate, i.e. two models for one specimen might predict generalist predator and specialist predator, or leaf litter foraging and epigaeic foraging. This variability might reflect morphological similarity among proximate aspects, resulting in model error, but it may also reflect ecological variability within species; for example predatory ants may supplement their diet with plant material or occasionally forage across strata. While it is difficult to strictly attribute prediction mismatches to model error or ecological variability, we suggest that model error is more readily identifiable when two models predict ecologies with no known affinities. Additionally, consensus votes can be assessed on a specimen-by-specimen basis: when the

consensus vote is less than 50%, meaning that the prediction is a result of a plurality of votes rather than a majority, confidence in that prediction is lower. This assessment, however, can be influenced by the number of classes; in our datasets, prediction accuracy was higher with niche aspects that had fewer classes. It is important to contextualize the number of possible classes with consensus votes.

The implementation of this pipeline requires a taxonomic group with both fossil and extant representatives with morphological continuity that allows for homologous trait measurements across time series. The application of extant trait data in extinct ecological estimation is best suited among lineages that exhibit a high degree of extant diversity relative to fossil samples: the more ecologies that the extant group occupies, the more likely it is that all potential ecological niches of the extinct group are represented. Predicted ecologies should also be evaluated in the context of other fossil evidence. For example, several extant ant taxa are primarily granivorous seed-eaters (Cole 1968; Plowes et al. 2013), thus the functional role of an extinct species could potentially be predicted as granivorous. However, while grasses first evolved in the early Cretaceous, grassland ecosystems did not develop broadly until later in the Cenozoic, making it unlikely that Mesozoic ants would have been granivorous (Stromberg 2011; Boyce and Lee 2017).

Ecological extinction and succession in the earliest ants

We recover broad consensus across models for hell ant ecological niche occupation: our models consistently predict haidomyrmecine taxa as leaf litter foraging or epigaeic ground-nesting predators, with few outliers (Figure 4). Our results contrast with previous hypotheses suggesting a primarily arboreal lifestyle among hell ants. Initial hypotheses were based on qualitative assessments of morphology (Barden and Grimaldi 2012), expected amber entrapment bias towards arboreal-associated species (Solórzano-Kraemer et al. 2015, 2018), and an assertion that hell ants' vertically aligned mandibles might have precluded the fine

manipulation of soil required to create ground nests (Dlussky 1996). The susceptibility of arboreal-associated species to extinction during cataclysmic events (Field et al. 2018) also provided a plausible explanation of the hell ants' demise. However, in addition to our own quantitative estimations of hell ant ecology, extant and fossilized behavioral evidence provide additional support for predicted ground and leaf litter habits among haidomyrmecines. Many extant trap-jaw ant species are capable of manipulating soil with their highly specialized mandibles, allowing for ground-nesting trap-jaw species (Cerquera and Tschinkel 2010). Soil nesting is also estimated as the ancestral state among all crown ants, though fossils have not yet been included in such reconstructions (Lucky et al. 2013). Additionally, two fossilized examples of hell ant prey reflect leaf litter and surficial habitats: a beetle larva in association with a *Linguamyrmex vladi* worker (Barden et al. 2017), likely reflecting a humid leaf litter habitat; and a cockroach relative *Caputoraptor elegans* in association with *Ceratomyrmex ellenbergeri* (Barden et al. 2020), possibly living in leaf litter or surficial strata, although arboreal habits have been proposed (Bai et al. 2018). This reconstructed nesting ecology of hell ants also aligns with proposed "extrinsic factors" related to the evolution of eusociality (Evans 1977).

While our results do not support the hypothesis of hell ant arboreality as a factor in their extinction, we do find support for specialized predation in several hell ant genera. Species with specialized diets are at higher risk of extinction during cataclysmic events due to the greater likelihood of their food sources' extinction and lack of flexibility in diet (Chichorro et al. 2022; Machado et al. 2022). While it is unclear whether haidomyrmecines went extinct prior to the KPg boundary or were lost during the mass extinction event, a specialized predatory diet may have been a factor in their demise.

Our comparison of ecomorphospace occupation in hell ants and in four monophyletic lineages with independent origins of trap-jaw mechanisms illustrate ecological coherence across deep time and distantly related lineages. Our reconstructions suggest that hell ants were functional analogs to many modern-day trap-jaw lineages in surficial and leaf litter arthropod

communities: solitary-foraging hunters seeking out prey across the forest floor and in interstitial leaf litter spaces. The morphological adaptations of modern-day trap-jaw workers necessitate solo foraging: rapid power-amplified closure of their specialized mandibles following the activation of elongate trigger setae in the path of mandible movement, subsequently stinging their prey. This specialized prey capture typically precludes group predation; workers individually subdue a single prey item before returning to the nest (Becker et al. 1989; Larabee and Suarez 2014). There are some morphological traits that support a trap-jaw mechanism in hell ants, including trigger hairs and a structurally-reinforced clypeal paddle at the point of mandible articulation (Barden & Grimaldi 2012; Barden et al. 2017). Moreover, there is direct paleoethological evidence of solitary foraging among hell ant workers (Barden et al. 2020).

Our paleoecological estimation allows for the recovery of repeated ecological niche occupation across lineages of predators. Hell ants occupied approximately 10% of hypothetical potential sampled ecomorphospace and yet radiated into leaf litter, surficial, and to a lesser degree, arboreal habitats in an ecomorphospace occupation that mirrors living lineages; hell ants entirely or at least partially overlap with each independent origin of extant trap jaw ants. Even as molecular-based divergence estimates place the origin of modern ants during the Cretaceous (Moreau et al. 2006; Borowiec et al. 2019), the earliest extant trap-jaw predators emerged later in the Cenozoic, from ~65 Ma in ponerines to ~35 Ma in *Strumigenys*, and after the last appearance of hell ants in the fossil record (Figure 3) (Ward et al. 2015; Booher et al. 2021; Fernandes et al. 2021). The last known hell ant fossil dates to 78 Ma in Campanian-age Canadian amber (McKellar et al. 2013). It is unclear precisely when hell ants went extinct, but the overlap of ecospace occupation between hell ants and the ponerine and dacetine lineages arising very soon after the KPg extinction may be a signature of faunal turnover in niche occupation. The extinction of hell ant lineages may have provided vacant ecospace that was filled by modern trap-jaw lineages. Additionally, while we included most known trap-jaw species in our extant ecospace reconstructions, fossil sampling remains much more limited; thus the full

ecospace occupation of hell ants was probably more broad than our current reconstruction suggests. The ecological breadth of the more than 1000 modern trap-jaw ant species (Bolton 2021) may represent echoes of their Cretaceous counterparts.

Faunal and ecological turnovers are a frequent feature of evolutionary history on Earth; the fossil record contains a plethora of examples (Sallan et al. 2011; Benson and Druckenmiller 2014; Moon and Stubbs 2020). We provide here a new quantitative framework for testing a variety of paleoecological hypotheses, including evaluations of ecology-based extinction risk, ecological succession in deep time, and competition between temporally and spatially proximate lineages. Our investigation of hell ant ecology generated a new test of ecology-linked extinction, and revealed a detailed ecological turnover in ecomorphospace occupation among temporally disjunct monophyletic lineages. By reconstructing the ecological community of the earliest ants, we find repeated lineage occupation of ecospace that is consistent with functional succession across Earth's last mass extinction event.

Acknowledgements

We thank Christine Johnson, Christine Lebeau, Morgan Hill, and Andrew Smith for facilitating access to specimens and imaging equipment at the American Museum of Natural History; Stefan Cover and David Lubertazzi for specimen access at the Museum of Comparative Zoology; and Eugenia Okonski and Ted Schultz for specimen access at the Smithsonian National Museum of Natural History. We thank two anonymous reviewers and The American Naturalist editors for suggestions which substantially improved this manuscript.

Funding*:* A portion of the initial work in collecting extant ant data and developing the model was funded by an Arthur James Boucot Research Grant from the Paleontological Society.

Competing Interest Statement: The authors declare that they have no competing interests.

Statement of Authorship

C.S., P.B. conceptualized the study; C.S., P.B. developed methodology and conducted statistical analyses; C.S., T.J., V.P., J.P.T., P.B. all contributed to data compilation and collection, data visualization, writing of the original draft, and reviews and edits of the final draft.

Ethics of the study: The fossil specimens used in this research are preserved primarily within Burmese amber. We affirm that all specimens were acquired prior to June 2017, pursuant to the proposed boycott of Burmese amber by the Society of Vertebrate Paleontologists (Rayfield et al. 2020). Some specimens are located in a private collection, while others are located in institutional museums: specimen repositories are indicated in the Supplementary Information associated with this manuscript, and we have provided photomicrographs of all specimens residing in a private collection. All data associated with this manuscript are available as Supplementary Information, including all morphometric measurements for privately-owned specimens.

Data and materials availability

All data and scripts needed to reproduce the analyses and evaluate the conclusions in the paper are present in the paper, Supplementary Information, and archived on the data repository Zenodo (doi: 10.5281/zenodo.7897553).

Literature Cited

Abràmoff, M. D., P. J. Magalhães, and S. J. Ram. 2004. Image processing with ImageJ. Biophotonics International 11(7):36-42.

Adler, D., D. Murdoch, O. Nenandic, S. Urbanek, M. Chen, A. Gebhardt, B. Bolker, G. Csardl, A. Strzeleckl, A. Senger, and R Core Team. 2021. Package “rgl”.

AntWeb. Version 8.64.2. California Academy of Science, online at https://www.antweb.org. Accessed February 2021.

Bai, M., R. G. Beutel, W. Zhang, S. Wang, M. Hörnig, C. Gröhn, E. Yan, X. Yang, and B. Wipfler. 2018. A new Cretaceous insect with a unique cephalo-thoracic scissor device. Current Biology 28(3):38-443.

Barden, P., and D. Grimaldi. 2012. Rediscovery of the bizarre Cretaceous ant *Haidomyrmex* Dlussky (Hymenoptera: Formicidae), with two new species. American Museum Novitates 2012(3755):1-16.

Barden, P., and D. A. Grimaldi. 2016. Adaptive radiation in socially advanced stem-group ants from the Cretaceous. Current Biology 26(4):515-521.

Barden, P., H. W. Herhold, and D. A. Grimaldi. 2017. A new genus of hell ants from the Cretaceous (Hymenoptera: Formicidae: Haidomyrmecini) with a novel head structure. Systematic Entomology 42(4):837-846.

Barden, P., V. Perrichot, and B. Wang. 2020. Specialized predation drives aberrant morphological integration and diversity in the earliest ants. Current Biology 30(19):3818-3824.

Barton, P.S., H. Gibb, A. D. Manning, D. B. Lindenmayer, and S. A. Cunningham. 2011. Morphological traits as predictors of diet and microhabitat use in a diverse beetle assemblage. Biological Journal of the Linnean Society 102:301–310.

Beckers, R., S. Goss, J. L. Deneubourg, and J. M. Pasteels. 1989. Colony size, communication, and ant foraging strategy. Psyche 96(3-4):239-256.

Benson, R. B., N. E. Campione, M. T. Carrano, P. D. Mannion, C. Sullivan, P. Upchurch, and D. C. Evans. 2014. Rates of dinosaur body mass evolution indicate 170 million years of sustained ecological innovation on the avian stem lineage. PLoS Biology 12(5):e1001853.

Benson, R.B. and P.S. Druckenmiller. 2014. Faunal turnover of marine tetrapods during the Jurassic–Cretaceous transition. Biological Reviews 89(1):1-23.

Bolton, B. 2021. An online catalog of the ants of the world. Available from https://antcat.org. (accessed July 2021)

Booher, D. B., J. C. Gibson, C. Liu, J. T. Longino, B. L. Fisher, M. Janda, N. Narula, E. Toulkeridou, A. S. Mikheyev, A. V. Suarez, and E. P. Economo. 2021. Functional innovation promotes diversification of form in the evolution of an ultrafast trap-jaw mechanism in ants. PLoS Biology 19(3):e3001031.

Borowiec, M. L., C. Rabeling, S. G. Brady, B. L. Fisher, T. R. Schultz, and P. S. Ward. 2019. Compositional heterogeneity and outgroup choice influence the internal phylogeny of the ants. Molecular Phylogenetics and Evolution 134:111-121.

Boyce, C. K., and J. E.Lee. 2017. Plant evolution and climate over geological timescales. Annual Review of Earth and Planetary Sciences 45:61-87.

Brady, S. G., T. R. Schultz, B. L. Fisher, and P. S. Ward. 2006. Evaluating alternative hypotheses for the early evolution and diversification of ants. Proceedings of the National Academy of Sciences 103(48):18172-18177.

Breiman L. 2001. Random Forests. Machine Learning 45:5-32.

Brown Jr, W. L. 1978. Contributions toward a reclassification of the Formicidae. Part VI. Ponerinae, tribe Ponerini, subtribe Odontomachiti. Section B. Genus *Anochetus* and bibliography. Studia Entomologica 20(1-4):549-652.

Cerquera, L. M., and W. R. Tschinkel. 2010. The nest architecture of the ant *Odontomachus brunneus*. Journal of Insect Science 10(1):64.

Chen, M., and G. P. Wilson. 2015. A multivariate approach to infer locomotor modes in Mesozoic mammals. Paleobiology 41(2):280-312.

Chen, M., C. A. Strömberg, and G. P. Wilson. 2019. Assembly of modern mammal community structure driven by Late Cretaceous dental evolution, rise of flowering plants, and dinosaur demise. Proceedings of the National Academy of Sciences 116(20):9931-9940.

Chichorro, F., F. Urbano, D. Teixeira, H. Väre, T. Pinto, N. Brummitt, X. He, A. Hochkirch, J. Hyvönen, L. Kaila, and A. Juslén. 2022. Trait-based prediction of extinction risk across terrestrial taxa. Biological Conservation 274:109738.

Cole Jr., A.C. 1968. *Pogonomyrmex* harvester ants. A study of the genus in North America. Page 38. Knoxville Tennessee: University of Tennessee Press.

Dickson, B. V., E. Sherratt, J. B. Losos, and S. E. Pierce. 2017. Semicircular canals in Anolis lizards: ecomorphological convergence and ecomorph affinities of fossil species. Royal Society Open Science 4(10):170058.

Dlussky, G. M. 1996. Ants (Hymenoptera: Formicidae) from Burmese amber. Paleontological Journal 30:449-454.

Dornhaus, A. and S. Powell. 2010. Foraging and defence strategies. Pages 210-230 in L. Lach, C.L. Parr, K.L. Abbott, eds. Ant Ecology.

Drumheller, S. K., and E. W. Wilberg, 2020. A synthetic approach for assessing the interplay of form and function in the crocodyliform snout. Zoological Journal of the Linnean Society 188(2):507-521.

Dunn, R. H., C. Cooper, J. Lemert, N. Mironov, and J. A. Meachen. 2019. Locomotor correlates of the scapholunar of living and extinct carnivorans. Journal of Morphology 280(8):1197-1206.

Engel, M. S., and D. A. Grimaldi. 2005. Primitive new ants in Cretaceous amber from Myanmar, New Jersey, and Canada (Hymenoptera: Formicidae). American Museum Novitates 2005(3485):1-24.

Ercoli, M. D., F. J. Prevosti, and A. Alvarez. 2012. Form and function within a phylogenetic framework: locomotory habits of extant predators and some Miocene Sparassodonta (Metatheria). Zoological Journal of the Linnean Society 165(1):224-251.

Evans, H.E. 1977. Commentary: extrinsic versus intrinsic factors in the evolution of insect sociality. BioScience 27(9):613-617.

Fedorov, A., R. Beichel, J. Kalpathy-Cramer, J. Finet, J.C. Fillion-Robin, S. Pujol, C. Bauer, D. Jennings, F. Fennessy, M. Sonka, and J. Buatti. 2012. 3D Slicer as an image computing platform for the Quantitative Imaging Network. Magnetic Resonance Imaging 30(9):1323-1341.

Fernandes, I. O., F. J. Larabee, M. L. Oliveira, J. H. Delabie, and T. R. Schultz. 2021. A global phylogenetic analysis of trap-jaw ants, *Anochetus* Mayr and *Odontomachus* Latreille (Hymenoptera: Formicidae: Ponerinae). Systematic Entomology 46:685-703.

Field, D.J., A. Bercovici, J.S. Berv, R. Dunn, D.E. Fastovsky, T.R. Lyson, V. Vajda, and J.A. Gauthier. 2018. Early evolution of modern birds structured by global forest collapse at the end-Cretaceous mass extinction. Current Biology 28(11):1825-1831.

Figueirido, B., A. Martín-Serra, and C. M. Janis. 2016. Ecomorphological determinations in the absence of living analogues: the predatory behavior of the marsupial lion (*Thylacoleo carnifex*) as revealed by elbow joint morphology. Paleobiology 42(3):508-531.

Figueirido, B., P. Palmqvist, J. A. Perez-Claros, and C. M. Janis. 2019. Sixty-six million years along the road of mammalian ecomorphological specialization. Proceedings of the National Academy of Sciences of the United States of America 116:12698–12703.

Frederickson, J. A., M. H. Engel, and R. L. Cifelli. 2018. Niche partitioning in theropod dinosaurs: Diet and habitat preference in predators from the Uppermost Cedar Mountain Formation (Utah, USA). Scientific Reports 8(1):1-13.

Gerry, S. P., J., Wang, and D. J. Ellerby. 2011. A new approach to quantifying morphological variation in bluegill *Lepomis macrochirus*. Journal of Fish Biology, 78:1023–1034.

Gibb, H., J. Stoklosa, D. I. Warton, A. M. Brown, N. R. Andrew, and S. A. Cunningham. 2015. Does morphology predict trophic position and habitat use of ant species and assemblages?. Oecologia 177(2):519-531.

Grimaldi, D., and D. Agosti. 2000. A formicine in New Jersey Cretaceous amber (Hymenoptera: Formicidae) and early evolution of the ants. Proceedings of the National Academy of Sciences 97(25):13678-13683.

Gronenberg, W., and B. Ehmer. 1996. The mandible mechanism of the ant genus *Anochetus* (Hymenoptera, Formicidae) and the possible evolution of trap-jaws. Zoology 99(3):153-162.

Hertel, F. 1995. Ecomorphological indicators of feeding behavior in recent and fossil raptors. The Auk 112(4):890-903.

Hoenle, P. O., J. E. Lattke, D. A. Donoso, C. von Beeren, M. Heethoff, S. Schmelzle, A. Argoti, L. Camacho, B. Ströbel, and N. Blüthgen. 2020. *Odontomachus davidsoni* sp. nov. (Hymenoptera, Formicidae), a new conspicuous trap-jaw ant from Ecuador. ZooKeys 948:75.

Hölldobler, B., and E. O. Wilson. 1990. The Ants. Harvard University Press. Cambridge, Massachusetts.

Jenkins, X. A., A. C. Pritchard, A. D. Marsh, B. T. Kligman, C. A. Sidor, and K. E. Reed. 2020. Using manual ungual morphology to predict substrate use in the Drepanosauromorpha and the description of a new species. Journal of Vertebrate Paleontology 40(5):1810058.

Lattke, J. E., and G. A. Melo. 2020. New haidomyrmecine ants (Hymenoptera: Formicidae) from mid-Cretaceous amber of Northern Myanmar. Cretaceous Research, 114:104502.

Larabee, F. J., and A. V. Suarez. 2014. The evolution and functional morphology of trap-jaw ants (Hymenoptera: Formicidae). Myrmecological News 20:25-36.

Lê, S., Josse, J., and F. Husson. 2008. FactoMineR: An R package for multivariate analysis. Journal of Statistical Software 25(1):1–18.

Liaw, A., and M. Wiener. 2018. RandomForest: Breiman and Cutler's random forests for classification and regression. R package version 4.

Losos, J. B. 1992. The evolution of convergent structure in Caribbean Anolis communities. Systematic Biology 41(4):403–420

Lucky, A., M. D. Trautwein, B. S. Guenard, M. D. Weiser, and R. R. Dunn. 2013. Tracing the rise of ants - out of the ground. PLOS One, 8(12):e84012.

Lungmus, J. K., and K. D. Angielczyk. 2021. Phylogeny, function and ecology in the deep evolutionary history of the mammalian forelimb. Proceedings of the Royal Society B 288(1949): 20210494.

Machado, F.F., L. Jardim, R. Dinnage, D. Brito, and M. Cardillo. 2022. Diet disparity and diversity predict extinction risk in primates. Animal Conservation.

McKellar, R. C., J. R. Glasier, and M. S. Engel. 2013. A new trap-jawed ant (Hymenoptera: Formicidae: Haidomyrmecini) from Canadian Late Cretaceous amber. The Canadian Entomologist 145(4):454-465.

Miller, E. T., S. K. Wagner, L. J. Harmon, and R. E. Ricklefs. 2017. Radiating despite a lack of character: ecological divergence among closely related, morphologically similar honeyeaters (Aves: Meliphagidae) co-occurring in arid Australian environments. The American Naturalist 189(2):E14-E30.

Meloro, C., and J. Louys. 2014. Ecomorphology of radii in Canidae: Application to fragmentary fossils from Plio-Pleistocene hominin assemblages. Acta Palaeontologica Polonica 60(4):795-806.

Meng, Q. J., D. M. Grossnickle, D. Liu, Y. G. Zhang, A. I. Neander, Q. Ji, and Z. X. Luo. 2017. New gliding mammaliaforms from the Jurassic. Nature 548(7667):291-296.

Moon, B.C. and T.L. Stubbs. 2020. Early high rates and disparity in the evolution of ichthyosaurs. Communications Biology 3(1):1-8.

Moreau, C. S., C. D. Bell, R. Vila, S. B. Archibald, and N. E. Pierce. 2006. Phylogeny of the ants: diversification in the age of angiosperms. Science 312(5770):101-104.

Moreau, C. S., and C. D. Bell. 2013. Testing the museum versus cradle tropical biological diversity hypothesis: phylogeny, diversification, and ancestral biogeographic range evolution of the ants. Evolution 67(8):2240-2257.

Mosimann, J. E. 1970. Size allometry: size and shape variables with characterizations of the lognormal and generalized gamma distributions. Journal of the American Statistical Association 65(330):930-945.

Palmqvist, P., D. R. Gröcke, A. Arribas, and R. A. Farina. 2003. Paleoecological reconstruction of a lower Pleistocene large mammal community using biogeochemical (δ13C, δ15N, δ18O, Sr: Zn) and ecomorphological approaches. Paleobiology 29(2):205-229.

Perrichot, V., S. Lacau, D. Néraudeau, and A. Nel. 2008. Fossil evidence for the early ant evolution. Naturwissenschaften 95(2):85-90.

Perrichot, V., B. Wang, M.S. Engel. 2016 Extreme morphogenesis and ecological specialization among Cretaceous basal ants. Current Biology 26(11):1468-1472.

Pigot, A. L., C. Sheard, E. T. Miller, T. P. Bregman, B. G. Freeman, U. Roll, N. Seddon, C. H. Trisos, B. C. Weeks, and J. A. Tobias. 2020. Macroevolutionary convergence connects morphological form to ecological function in birds. Nature Ecology & Evolution, 4(2):230-239.

Plowes, N.J.R., R.A Johnon, and B. Holldobler. 2013. Foraging behavior in the ant genus *Messor* (Hymenoptera: Formicidae: Myrmicinae). Myrmecological News 18:33-49.

R Core Team. 2021. R: A language and environment for statistical computing. R Foundation for Statistical Computing.

Rayfield, E. J., J. M. Theodor, and P. D. Polly. 2020. Fossils from conflict zones and reproducibility of fossil-based scientific data. Society of Vertebrate Paleontology (SVP), letter, 21/04/2020.

Rector, A. L., and M. Vergamini. 2018. Forelimb morphology and substrate use in extant Cercopithecidae and the fossil primate community of the Hadar sequence, Ethiopia. Journal of Human Evolution 123:70-83.

Sallan, L.C., T.W. Kammer, W.I. Ausich, and L.A. Cook. 2011. Persistent predator–prey dynamics revealed by mass extinction. Proceedings of the National Academy of Sciences 108(20):8335-8338.

Saunders, M. B., and R. M. R. Barclay. 1992. Ecomorphology of insectivorous bats: A test of predictions using two morphologically similar species. Ecology 73(4):1335–1345.

Schneider, C. A., W. S. Rasband, and K. W. Eliceiri. 2012. NIH Image to ImageJ: 25 years of image analysis. Nature Methods 9(7):671–675.

Solórzano Kraemer, M. M., A. S. Kraemer, F. Stebner, D. J. Bickel, and J. Rust. 2015. Entrapment bias of arthropods in Miocene amber revealed by trapping experiments in a tropical forest in Chiapas, Mexico. PloS One 10(3):e0118820.

Solórzano Kraemer, M. M., X. Delclòs, M. E. Clapham, A. Arillo, D. Peris, P. Jäger, F. Stebner, and E. Peñalver. 2018. Arthropods in modern resins reveal if amber accurately recorded forest arthropod communities. Proceedings of the National Academy of Sciences 115(26):6739–6744.

Sosiak, C. E., and P. Barden. 2021. Multidimensional trait morphology predicts ecology across ant lineages. Functional Ecology 35(1):139-152.

Sosiak, C. E., T. Janovitz, V. Perrichot, J. P. Timonera, and P. Barden. 2023. Data for: Trait-based paleontological niche prediction recovers extinct ecological breadth of the earliest specialized ant predators. Zenodo Data Repository, doi: 10.5281/zenodo.7897553.

Strauss, R.E. 2010. Discriminating groups of organisms. Pages 73-91 in A. Elewa, ed. Morphometrics for nonmorphometricians. Springer, Berlin, Germany.

Strömberg, C. A. 2011. Evolution of grasses and grassland ecosystems. Annual Review of Earth and Planetary Sciences, 39:517-544.

Ward, P. S., S. G. Brady, B. L. Fisher, and T. R. Schultz. 2015. The evolution of myrmicine ants: phylogeny and biogeography of a hyperdiverse ant clade (Hymenoptera: Formicidae). Systematic Entomology 40(1):61-81.

Wei, T., V. Simko, M. Levy, Y. Xie, Y. Jin, and J. Zemla. 2017. Package 'corrplot'. Statistician, 56:316–324.

Weiser, M. D., and M. Kaspari. 2006. Ecological morphospace of New World ants. Ecological Entomology 31(2):131-142.

Wickham, H. 2016. ggplot2: Elegant Graphics for Data Analysis. Springer-Verlag New York.

Williams, E. E. 1972. 3. The Origin of Faunas: Evolution of lizard congeners in a complex island fauna: A trial analysis. Pages 47-89 in T. Dobzhansky, M.K. Hecht and W.C. Steere eds. Evolutionary Biology, Meredith Corporation.

Wilson, E. O., F. M. Carpenter, and W. L. Brown. 1967. The first Mesozoic ants. Science 157(3792):1038-1040.

Wilson, E. O. 1987. Causes of ecological success: the case of the ants. Journal of Animal Ecology 56(1):1-9.

Wilson, E. O. 1987. The earliest known ants: an analysis of the Cretaceous species and an inference concerning their social organization. Paleobiology 13(1):44-53.

Wilson, E. O., and B. Hölldobler. 2005. The rise of the ants: a phylogenetic and ecological explanation. Proceedings of the National Academy of Sciences 102(21):7411-7414.

Yates, M. L., N. R. Andrew, M. Binns, and H. Gibb. 2014. Morphological traits: Predictable responses to macrohabitats across a 300 km scale. PeerJ, 2:e271.

Yates, M., and N. R. Andrew. 2011. Comparison of ant community composition across different land-use types: Assessing morphological traits with more common methods. Australian Journal of Entomology 50(2):118-124.

Tables

Table 1. All morphological traits measured, with description of measurements taken, and known ecological significance of traits.

TRAIT	DESCRIPTION OF MEASUREMENT	KNOWN ECOLOGICAL SIGNIFICANCE
Head width (HW)	Taken in frontal view along widest axis of head capsule excluding eyes	Mandibular musculature of workers (Kaspari 1993); size of spaces workers can move through (Sarty et al. 2006)
Head length (HL)	Medially from anterior margin of clypeus to vertex of head capsule in frontal view	Size of spaces workers can move through (Kaspari and Weiser 1999)
Eye length (EL)	Measured along longest axis of eye	Foraging behaviour and foraging period (Weiser and Kaspari 2006)
Mandible length (lateral profile view) (MLP)	From point of insertion to apical-most tooth of mandible	Diet (Fowler et al. 1991)
Anteroposterior eye position (3 measurements taken) (LHL; ELA; ELP)	Taken in lateral view: length from midpoint of eye to anterior clypeal margin (ELA); length of head from midpoint of eye to posterior margin (ELP); total lateral head length (LHL) used to calculate eye position ratios	Foraging and diet (Fowler et al. 1991); habitat stratum (Gibb and Parr 2013)
Dorsoventral eye position (3 measurements taken) (HH; EHD; EHV)	Taken in lateral view: height of head from midpoint of eye to dorsal margin of head (EHD); height of head from midpoint of eye to ventral margin of head (EHV); total head height (HH) used to calculate eye position ratios	Related to foraging and diet (Fowler et al. 1991); habitat stratum occupied (Gibb and Parr 2013)
Mandible length (frontal view) (MLF)	From point of clypeal insertion to apical-most tooth of mandible	Diet (Fowler et al. 1991)
Scape length (SL)	From antennal socket to distal margin of scape	Chemosensory; detection of pheromone trails (Weiser and Kaspari 2006)
Weber's length (WL)	Taken in lateral view from the anterodorsal margin of the pronotum to the posteroventral margin of the mesosoma	Established proxy for worker body size (Weber 1938)

Procoxal length (PL)	From articulation point with propleuron to the distal tip of the procoxa	N/A
Mesosoma height (MH)	Taken at a right angle to Weber's length from the ventral margin of propleuron to dorsal margin of pronotum	N/A
Pronotal width (PW)	Measured at the widest point of the pronotum when viewed dorsally	Body mass of workers (Kaspari and Weiser 1999)
Metafemur length (ML)	Measured from articulation point with trochanter to distal tip of the metafemur	Foraging speed and habitat complexity (Feener et al. 1988)

Table 2. Ecological niche aspect binning abbreviations, definitions, and exemplar taxa.

BINNING DESIGNATOR	DEFINITION	EXEMPLAR TAXA
	FUNCTIONAL ROLE	
GP	Generalist predator – broad taxonomic diet	*Odontomachus; Diacamma; Harpegnathos*
SP	Specialist predator – obligate feeding on specific taxon (e.g. termites)	*Acanthostichus; Megaponera; Simopelta*
Om	Omnivorous – prey items, plant matter, etc.	*Paraponera; Camponotus; Iridomyrmex*
Py	Phytophagous – extrafloral nectaries, herbivory, etc.	*Pseudomyrmex; Tetraponera; Myrmelachista*
Fg	Fungus-growing	*Cyphomyrmex; Trachymyrmex; Atta*
Tr	Trophobiotic – symbiotic relationship with other insects (homopteran secretions, etc.)	*Acropyga; Melissotarsus; Rhopalomastix*
Gn	Granivorous – seed-harvesting	*Acanthomyrmex; Pogonomyrmex; Veromessor*
Mh	Mushroom-foraging	*Euprenolepis*
	NESTING NICHE	
Cn	Carton-nesting – structured nests from plant material in trees and shrubs	*Oecophylla; Azteca; Liometopum*

Gr	Ground-nesting – nests in dirt mounds, under stones, rock cracks, etc.	*Platythyrea; Formica; Pheidole*
Lg	Lignicolous – nests in twig and tree cavities	*Pseudomyrmex; Simopone; Cylindromyrmex*
Ll	Leaf litter-nesting – nests in leaf litter interstitial space, rotten wood, etc.	*Strumigenys; Discothyrea; Typhlomyrmex*
Sb	Subterranean-nesting	*Leptanilloides; Leptanilla*
	FORAGING NICHE	
Ab	Arboreal – in and on trees and shrubs	*Daceton; Tetraponera; Crematogaster*
CR	Column-raiding – cooperative, nomadic or raiding predation	*Simopelta; Dorylus; Eciton*
Eg	Epigaeic – active foraging on the ground surface	*Leptomyrmex; Rhytidoponera; Myrmecocystus*
Ll	Leaf litter – within interstitial spaces in leaf litter	*Discothyrea; Amblyopone; Heteroponera*
Sb	Subterranean – underground	*Acropyga*

Table 3. Out-of-bag accuracies (given in percentages) for each Random Forest model constructed.

	NESTING NICHE	FORAGING NICHE	FUNCTIONAL ROLE	ECOMORPH
COMPLETE MORPHOMETRIC DATASET				
Linear trait measurements	85.77	83.63	85.88	81.78
Shape ratio measurements	82.92	85.05	80.92	79.84
Log-shape variable measurements	88.61	88.97	82.06	82.56
SUBSET OF COMPLETE MORPHOMETRIC DATASET				
Linear trait measurements	85.41	82.92	80.53	81.78
Shape ratio measurements	80.07	81.14	82.06	77.91
Log-shape variable measurements	86.83	84.34	83.21	81.78

Figure Legends

Figure 1. Diagrammatic workflow of predictive model development and testing. A comprehensive morphometric dataset of extant ants was compiled; species were binned according to various ecological niche aspects based on surveys of the literature. Random Forest models were then trained on subsets of the original dataset. Homologous traits were measured on fossil ant specimens; when available, traits were measured from CT reconstructions, and otherwise were measured under light microscopy. Finally, the pre-trained Random Forest models were used to predict extinct ecology from fossil morphometric datasets.

Figure 2. Consensus model votes for niche aspect predictions. Each species' niche aspect predictions are represented by six models derived from alternate datasets; from top left, clockwise: linear functional measurements; log-shape variable functional measurements; shape ratio functional measurements; shape ratio homologous measurements; log-shape variable homologous measurements; linear homologous measurements. Taxonomic sampling includes described (named) taxa as well as putative morphospecies. Alternate specimens of the same species are denoted with superscripts, *denotes specimens included through CT-scan reconstruction data. All model votes are available in Tables S4-51; full specimen information is available in Table S3.

Figure 3. Ecospace occupation of haidomyrmecine and extant specialist predator lineages. (Top left) Subfamily-level time-calibrated phylogeny of ants with divergence dates from Borowiec et al. (2019), Haidomyrmecinae and extant lineages denoted with colored bars; haidomyrmecine range derived from oldest and youngest deposit ages, extant ranges based on available crown age estimations for each lineage: Ponerinae – *Anochetus* + *Odontomachus* (Fernandes et al. 2021); Myrmicinae – *Strumigenys* (Booher et al. 2021); Myrmicinae – dacetine trap-jaws (Ward et al. 2015). No divergence date estimates are available for the formicine trap-jaw genus *Myrmoteras*. (Right) Lineage-specific ecomorphological niche occupations. Each colored cube represents a unique occupied niche. Hashed cubes in

haidomyrmecine ecospace indicate “maximum” hypothetical niche occupation based on all unique combinations estimated across all six random forest models while remaining cubes reflect only the majority aspect from the linear functional measurement model. All extant ecospaces compiled from literature. (Bottom left) Within-lineage ecological disparity calculated as average pairwise distance between each unique three-dimensional occupation. Maximum and minimum haidomyrmecine values represent alternate niche occupations described in the right panel. Ecological disparity values are listed in Table S52.

Figure 4. Reconstruction of the putative nesting and predatory foraging habits of the hell ant *Linguamyrmex vladi*. Artist: John Paul Timonera.

Figure 1

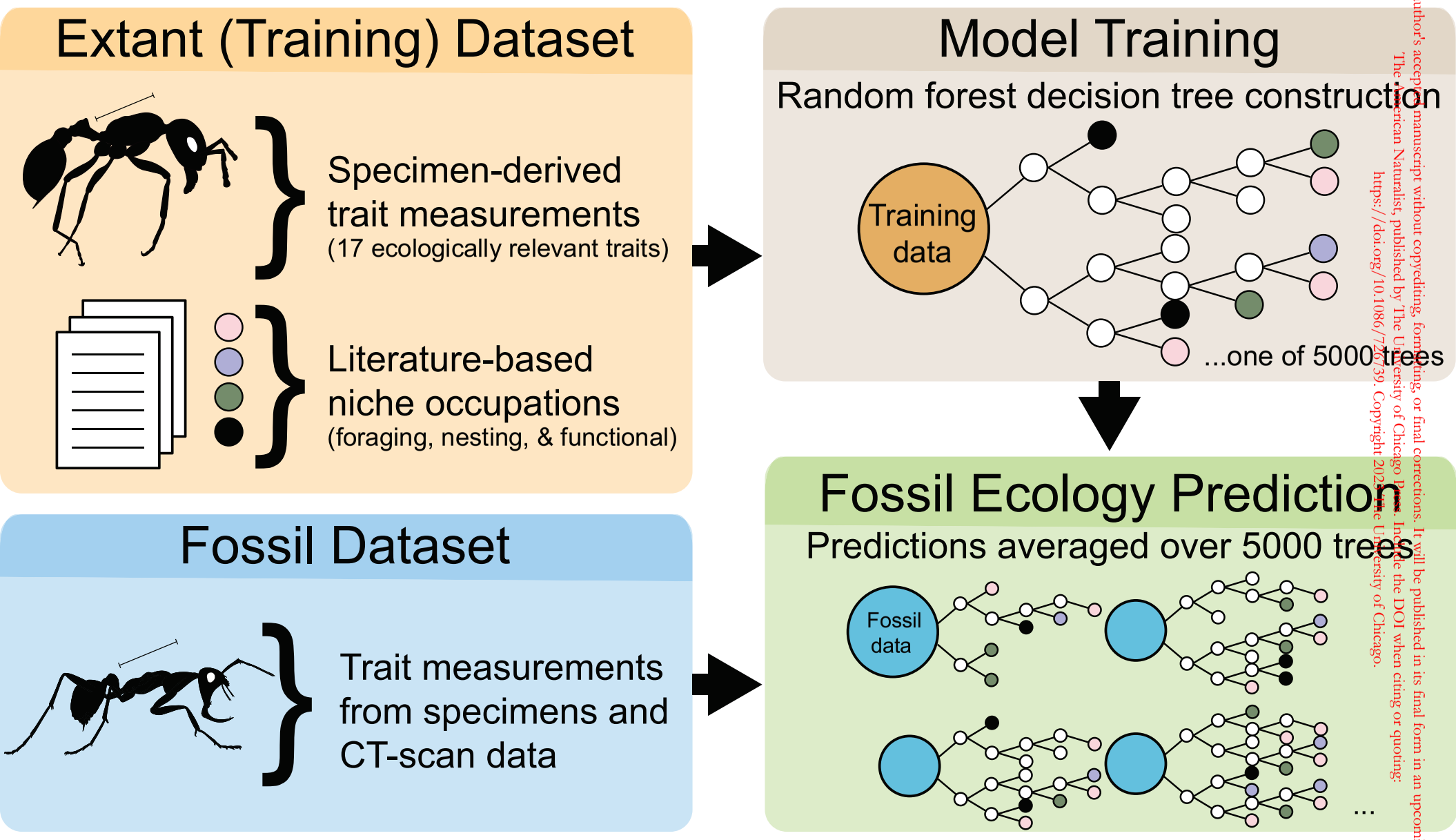

Figure 2

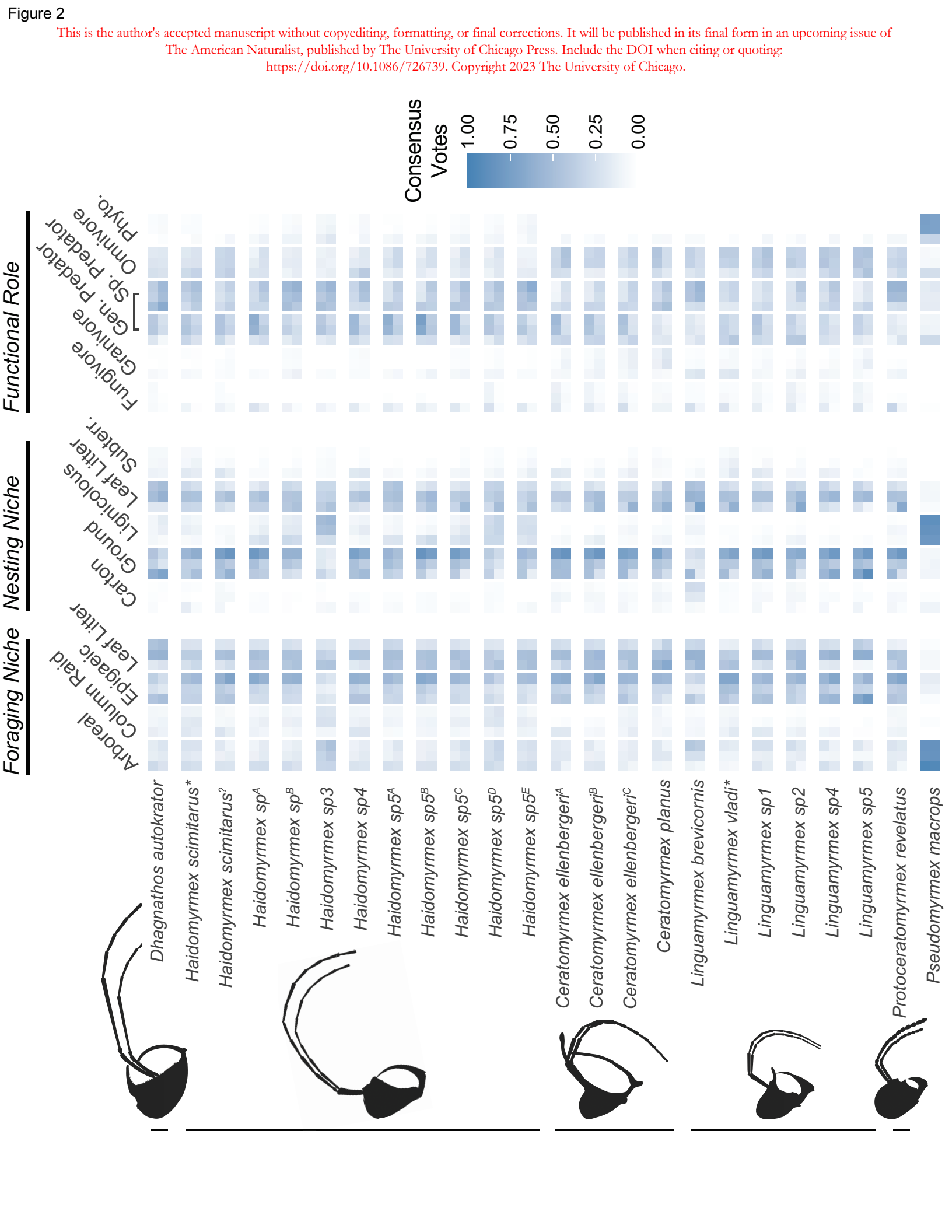

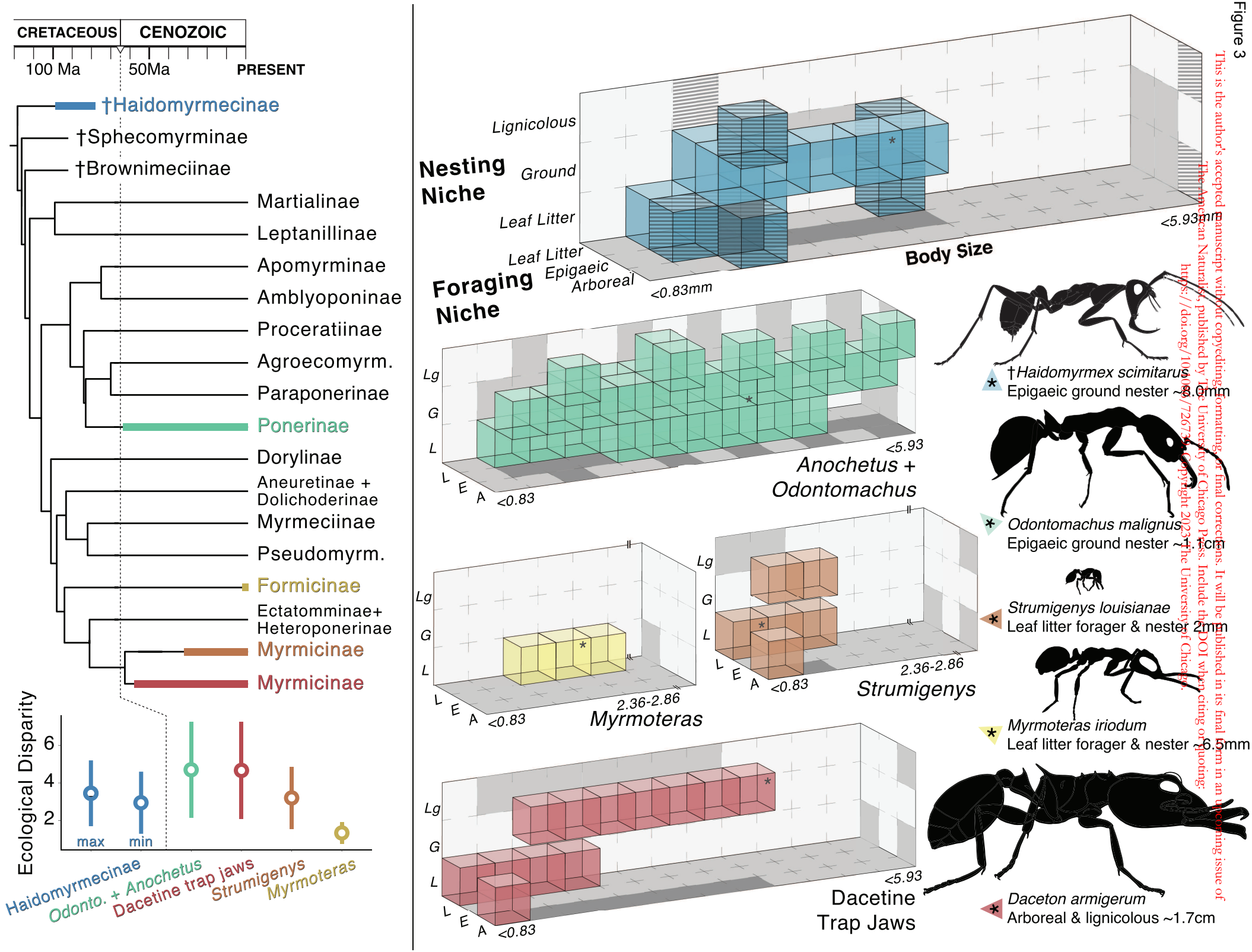

Figure 3

Figure 4

Supplementary Information for: Trait-based paleontological niche prediction recovers extinct ecological breadth of the earliest specialized ant predators

Authors: Christine Sosiak*[1], Tyler Janovitz[2], Vincent Perrichot[3], John Paul Timonera[4], Phillip Barden[1,5]

Affiliations: 1. Federated Department of Biological Sciences, New Jersey Institute of Technology; 2. Foundation Medicine Inc.; 3. Géosciences Rennes, Université de Rennes, CNRS; 4. Biological Sciences Program, St. Mary's University; 5. Division of Invertebrate Zoology, American Museum of Natural History

***Corresponding author:** Christine Sosiak, ces43@njit.edu

Keywords: paleoecology; ants; morphology; machine learning

Methods – Homologous versus functional morphology of hell ants

Most hell ant traits were distinguished as homologous to extant species; however, because haidomyrmecine cranial morphology is highly modified, eye position is difficult to assess in the context of modern ant variation. Extant ants (and most extinct ants, including the Dominican *Pseudomyrmex* fossil) have a prognathous head posture, in which the long axis of the head is held parallel to the ground with the oral opening pointing anteriad. In many other insect taxa, such as wasps and grasshoppers, the head is held in a hypognathous posture; the long axis of the head is held perpendicular to the ground, with the oral opening positioned ventrally. A hypognathous-like head posture is also present in hell ants, a configuration not seen in any extant ant. This difference in head posture means that, interpreted strictly on the basis of homology, the dorsoventral axis of the extant ant head is the anteroposterior axis of the hell ant head, and vice versa; that eye positioning along each axis is similarly swapped. When interpreted this way, the eye position of the hell ant is more similar to many *Camponotus* species: positioned extremely posteriorly and more dorsally.

Functionally, however, the hell ant would have been moving with its head held hypognathously, as evidenced by fossilized posture as well as preserved predation (Perrichot et al 2008; Barden & Grimaldi 2012; Perrichot et al. 2016; Barden et al. 2020) thus the functional anteroposterior axis of the hell ant head would be from its clypeal protrusion or horn to the occipital foramen, rather than the homologous anteroposterior axis of the head running perpendicular to the ground from vertex to oral opening. Considering that our question is a question of functional ecology - what is the ecological occupation of hell ants? - we measured traits related to eye position both functionally and homologously, to incorporate this possible variation (Figures S1, S2).

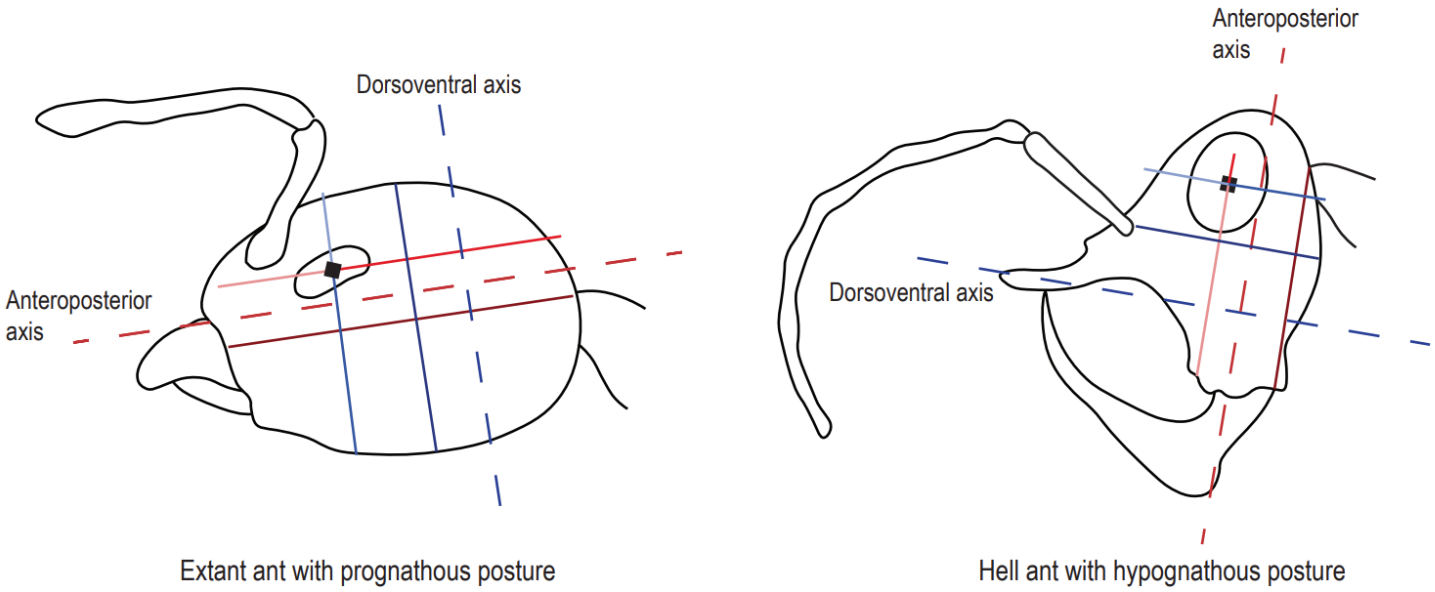

Figure S1.
Eye positioning measurements consistent with homologous morphology.

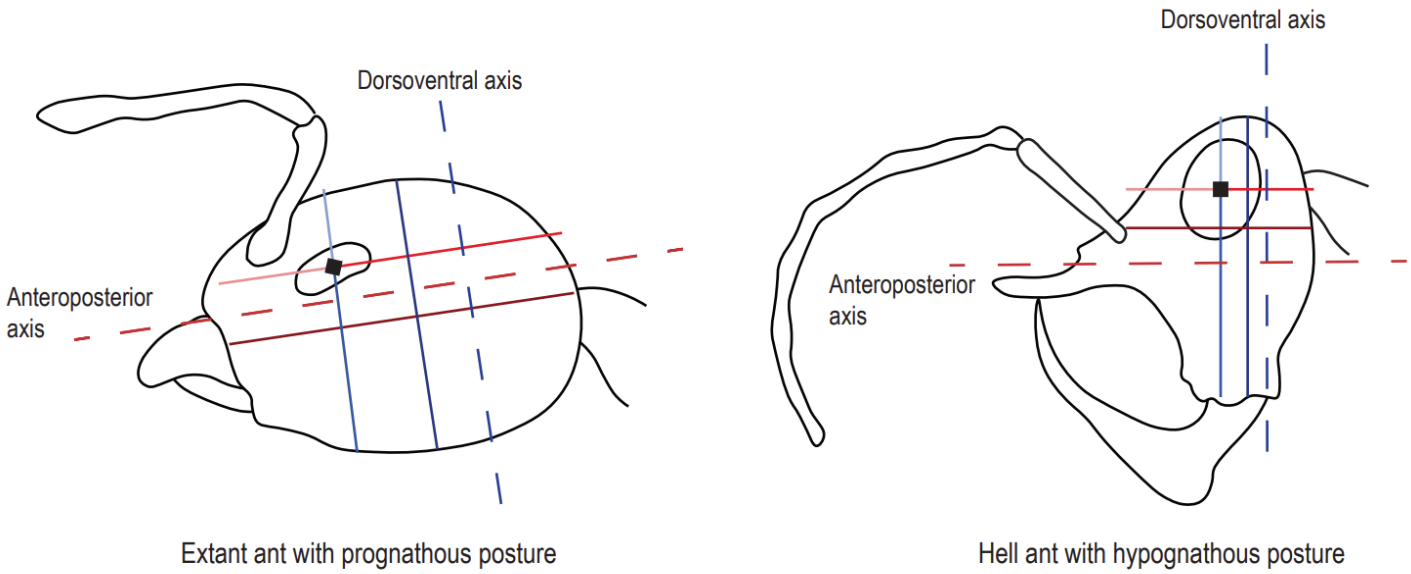

Figure S2.
Eye positioning measurements consistent with functional morphology.

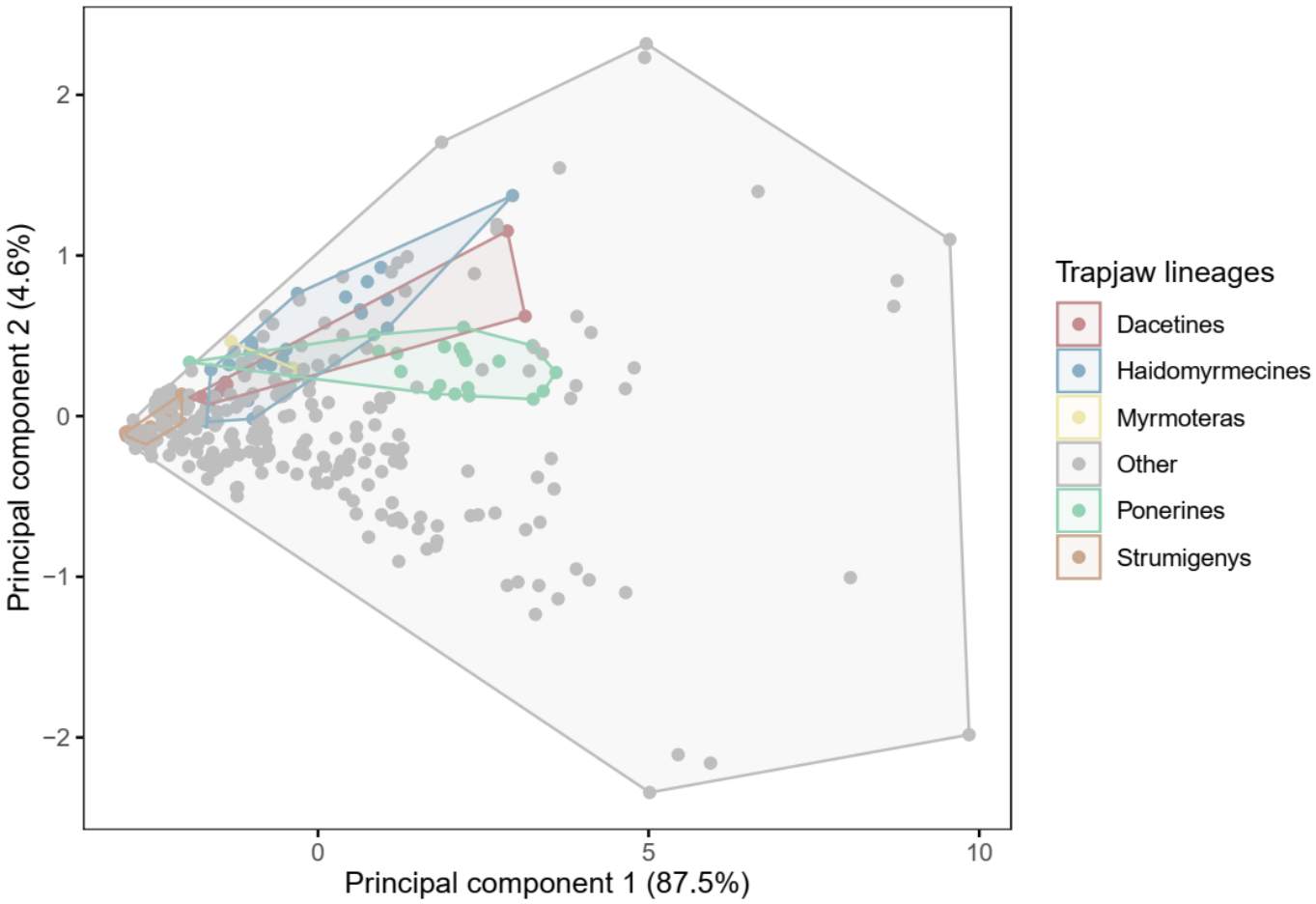

Figure S3.
Principal component analysis of extant and extinct morphospace using raw trait measurements. The morphospace of each lineage with an independent origin of trap-jaw mechanics is delineated.

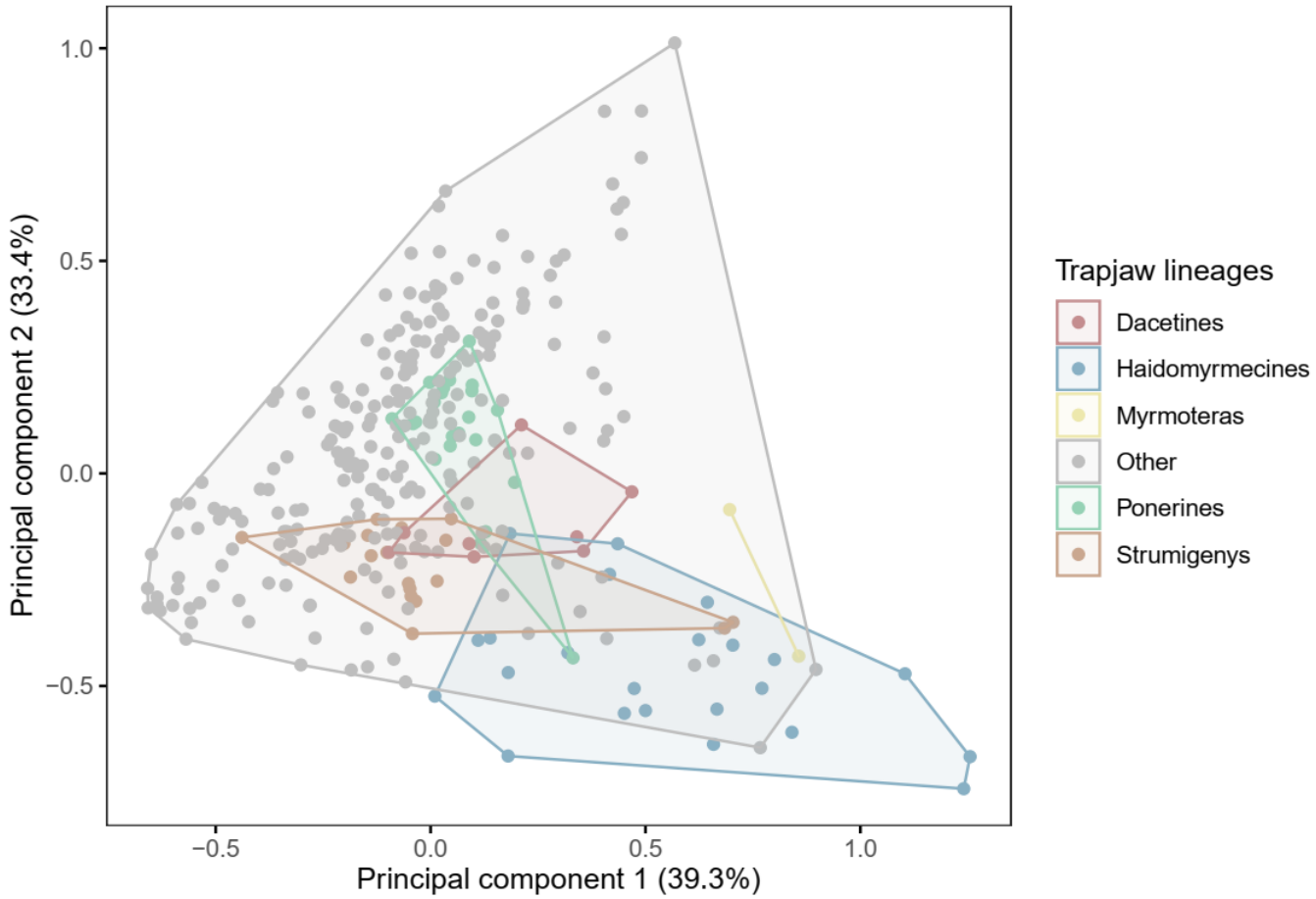

Figure S4.
Principal component analysis of extant and extinct morphospace using shape ratio measurements. The morphospace of each lineage with an independent origin of trap-jaw mechanics is delineated.

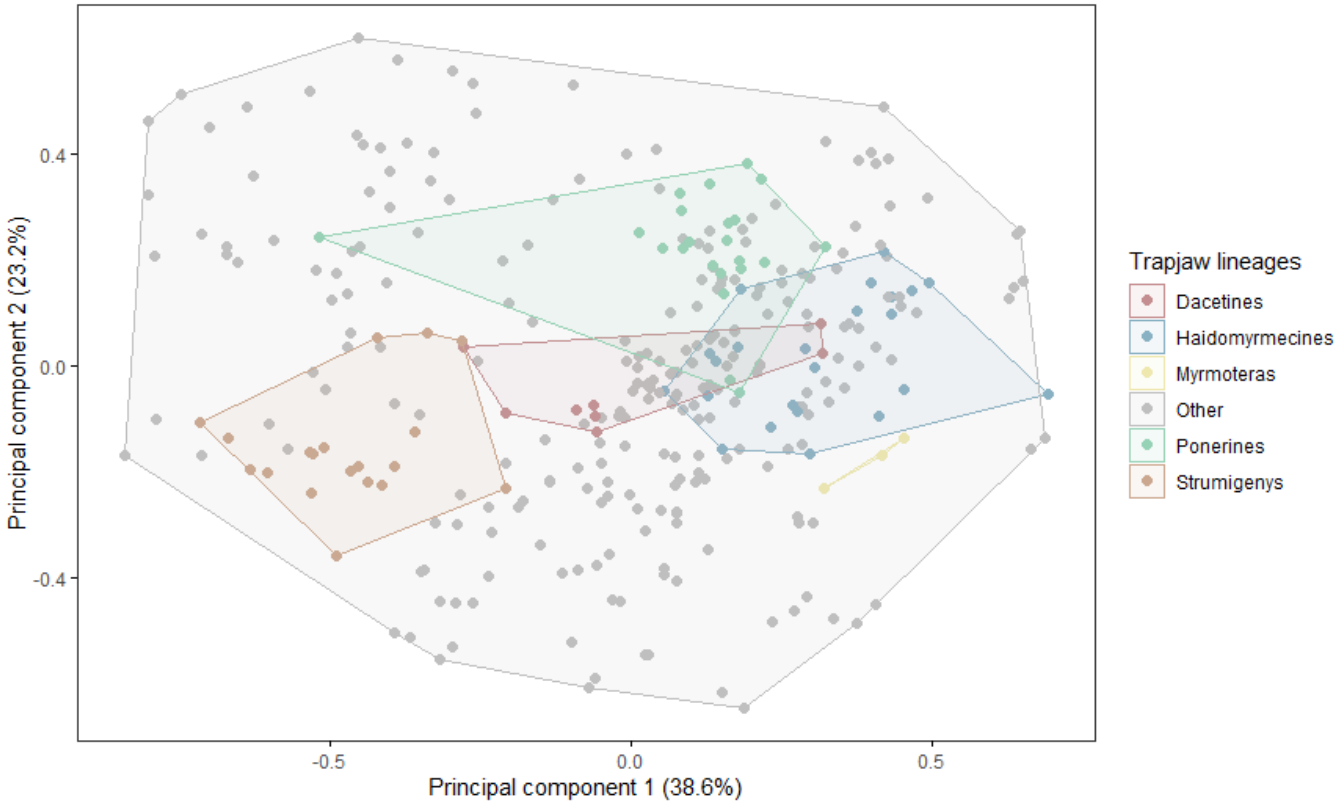

Figure S5.
Principal component analysis of extant and extinct morphospace using log-shape variable measurements. The morphospace of each lineage with an independent origin of trap-jaw mechanics is delineated.

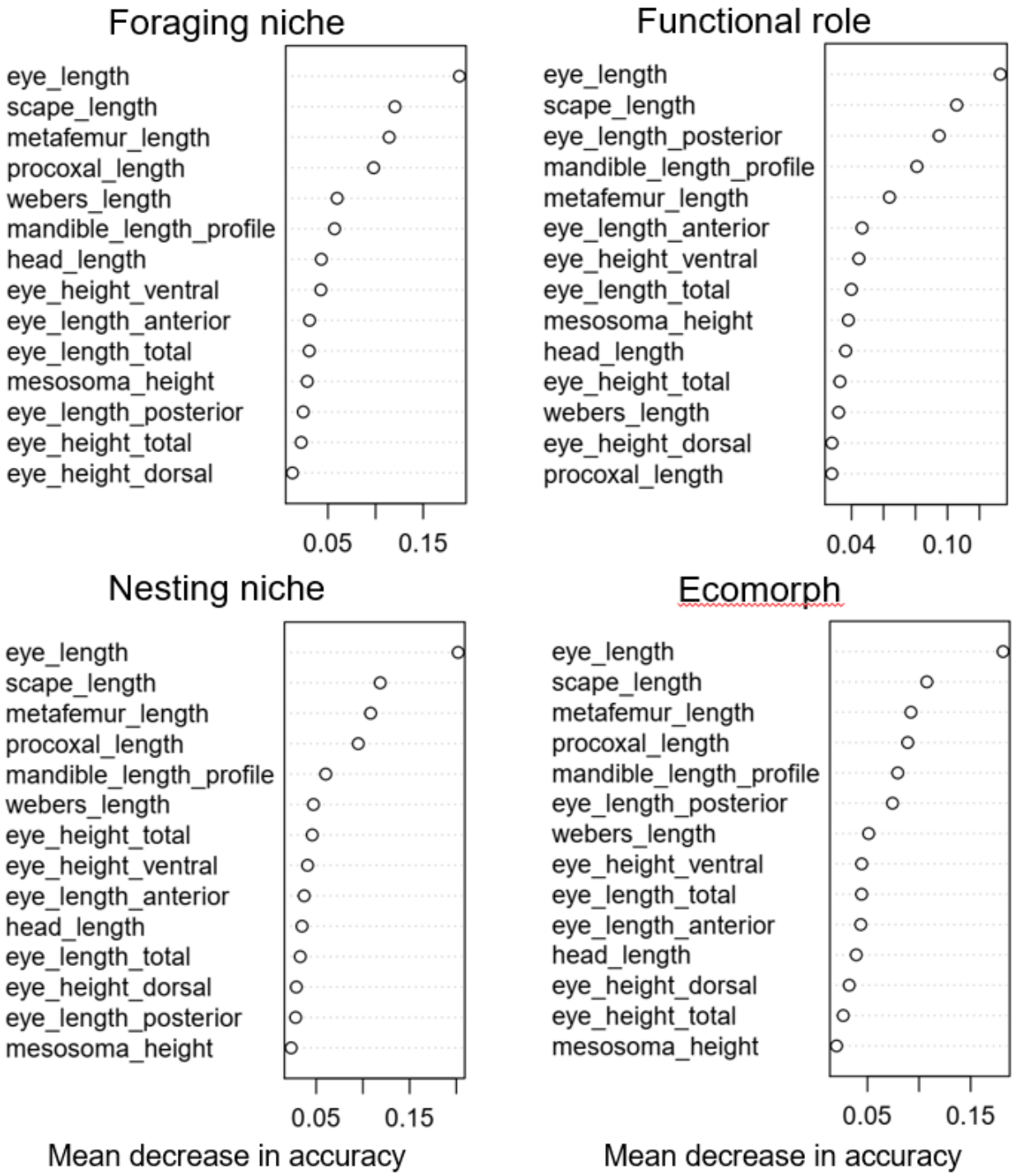

Figure S6.
Variable importance plots for each Random Forest classification model (foraging niche; functional role; nesting niche; ecomorph syndrome) using linear trait measurement data. Variable importance is calculated as the mean decrease in accuracy across splits when the variable was eliminated; a higher decrease in accuracy when that variable was omitted indicates greater importance to the model.

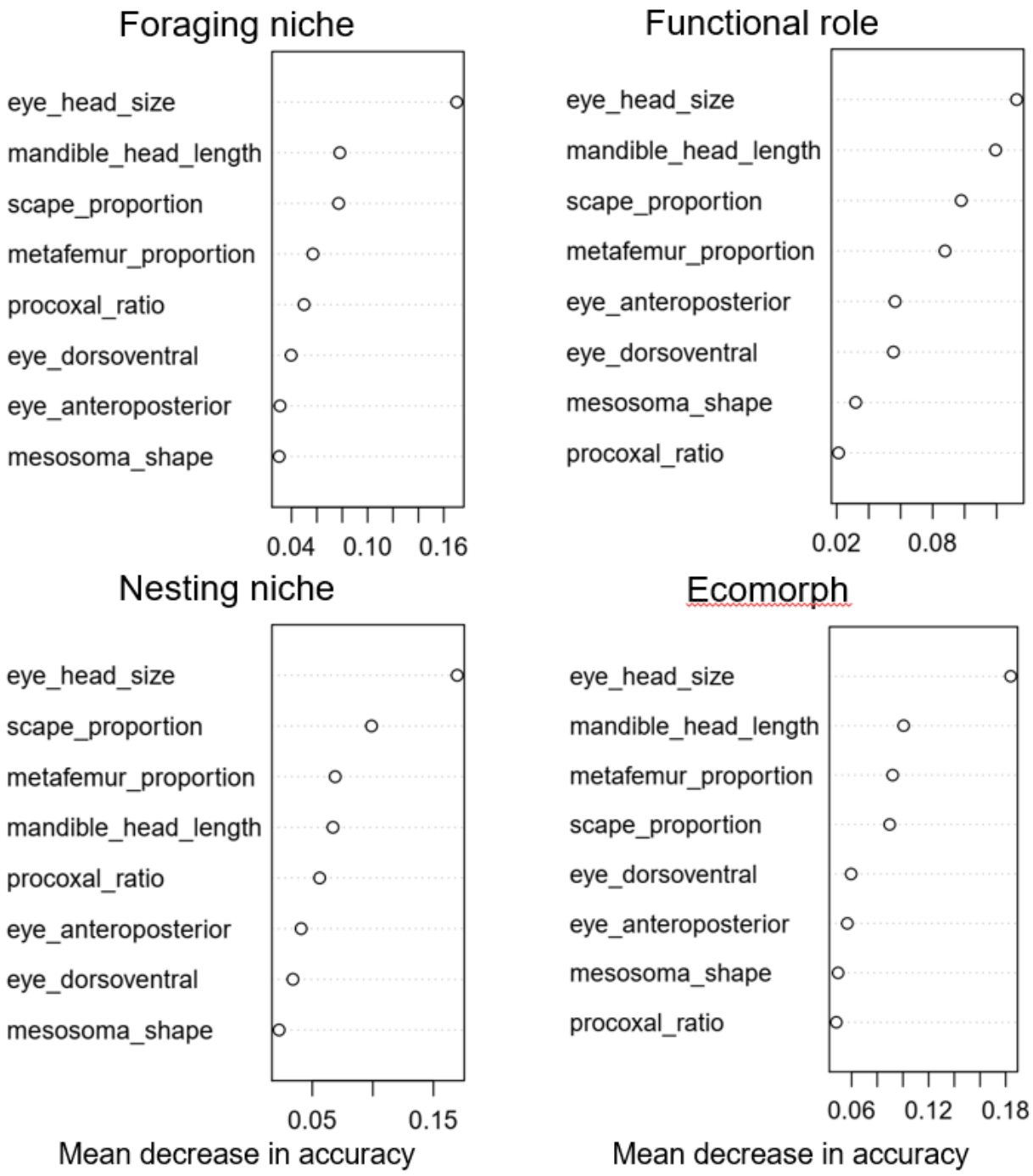

Figure S7.
Variable importance plots for each Random Forest classification model (foraging niche; functional role; nesting niche; ecomorph syndrome) using shape ratio measurement data. Variable importance is calculated as the mean decrease in accuracy across splits when the variable was eliminated; a higher decrease in accuracy when that variable was omitted indicates greater importance to the model.

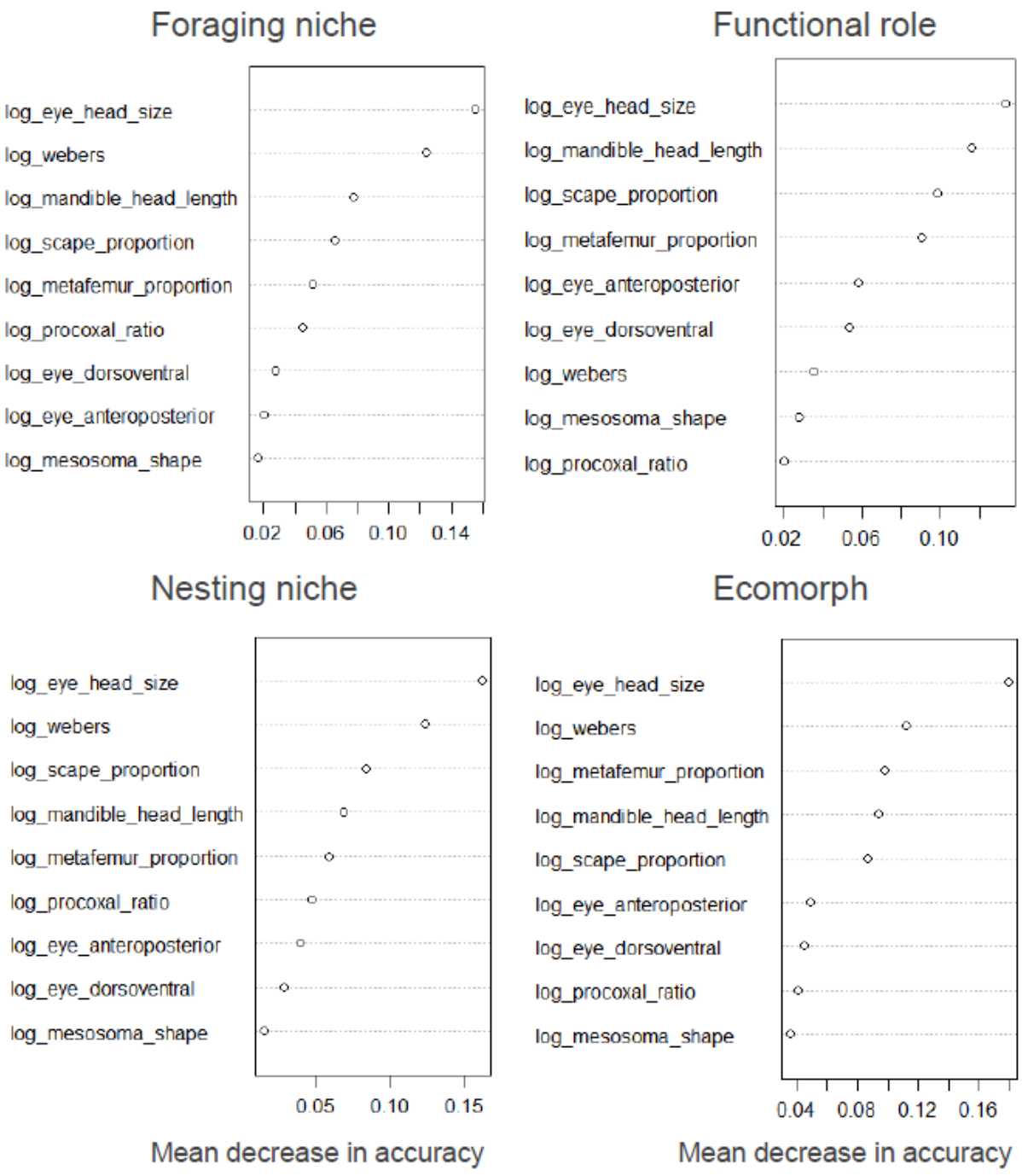

Figure S8.
Variable importance plots for each Random Forest classification model (foraging niche; functional role; nesting niche; ecomorph syndrome) using log-shape variable measurement data. Variable importance is calculated as the mean decrease in accuracy across splits when the variable was eliminated; a higher decrease in accuracy when that variable was omitted indicates greater importance to the model.

Trait	Formula	Interpretation
Head shape (HS)	HW/HL	Larger value = more boxy, square head Smaller value = more elongate along anteroposterior axis
Procoxal proportion (PP)	PL/WL	Larger value = procoxa longer in comparison to body length Smaller value = procoxa shorter in comparison to body length
Eye proportion (EP)	EL/HL	Larger value = eyes large in comparison to head Smaller value = eyes small in comparison to head
Pronotum expansion (PE)	PW/WL	Larger value = pronotum laterally expanded in relation to body size Smaller value = pronotum laterally narrow in relation to body size
Pronotum flattening (PF)	PW/MH	Larger value = pronotum broad and dorsoventrally flattened Smaller value = pronotum narrow and dorsoventrally expanded
Mesosoma shape (MS)	MH/WL	Larger value = overall elongate narrow body Smaller value = overall stocky squarish body
Mandible curvature (MC)	MLP/MLF	Larger value = low degree of mandible curvature Smaller value = high degree of mandible curvature
Mandible proportion (MP)	MLP/HL	Larger value = elongate mandibles in comparison with head size Smaller value = short mandibles in comparison with head size
Dorsoventral eye position (DEP)	EHD/HH	Larger value = eye positioned more ventrally Smaller value = eye positioned more dorsally
Anteroposterior eye position (AEP)	ELA/LHL	Larger value = eye positioned more posteriorly Smaller value = eye positioned more anteriorly
Scape proportion (SP)	SL/HL	Larger value = scape elongate in comparison with head size Smaller value = scape short in comparison with head size
Metafemur proportion (MeP)	ML/WL	Larger value = elongate leg in relation to body size Smaller value = shorter leg in relation to body size

Table S1.
Shape ratios of traits measured, formulae for calculation, and interpretation of ratio value.

Ecomorph designation based on granular binnings	Functional role binnings collapsed	Final ecomorph syndromes
fg_gr_eg	om_gr_eg	**Ground or leaf litter-nesting epigaeic omnivore** om_grll_eg Exemplars: *Camponotus; Dinoponera; Aphaenogaster*
gn_gr_eg		
mh_gr_ll	om_gr_ll	
om_gr_eg	om_gr_eg	
om_gr_ab	om_gr_ab	
om_gr_ll	om_gr_ll	
om_ll_eg	om_ll_eg	
gn_leaf	om_leaf	**Leaf litter omnivore** om_leaf Exemplars: *Aneuretus; Acanthomyrmex; Cyphomyrmex*
om_leaf		
om_lg_ab	om_lg_ab	**Lignicolous arboreal omnivore** om_lg_ab Exemplars: *Pseudomyrmex; Cataulacus; Cephalotes*
py_lg_ab		
tr_lg_ab		
om_cn_ab	om_cn_ab	**Carton-nesting arboreal omnivore** om_cn_ab Exemplars: *Crematogaster; Oceophylla; Azteca*
om_cn_eg	om_cn_eg	
om_sub	om_sub	**Subterranean omnivore** om_sub Exemplars: *Acropyga*
gp_gr_eg	pred_gr_eg	**Ground-nesting epigaeic or leaf litter predator** pred_gr_egll Exemplars: *Odontomachus; Diacamma; Harpegnathos*
sp_gr_eg	pred_gr_ll	
gp_gr_ll		
gp_leaf	pred_leaf	**Leaf litter predator** pred_leaf Exemplars: *Hypoponera; Mystrium; Strumigenys*
sp_leaf		
sp_lg_ab	pred_lg_ab	**Lignicolous arboreal predator** pred_lg_ab Exemplars: *Simopone; Cylindromyrmex; Daceton*
gp_lg_ab		
gp_ll_cr	pred_ll_cr	**Column-raiding predator** pred_cr Exemplars: *Simopelta; Neivamyrmex; Cheliomyrmex*
gp_sb_cr	pred_sb_cr	
sp_sb_cr		

sp_gr_cr	pred_gr_cr	
gp_ll_eg sp_ll_eg	pred_ll_eg	**Leaf litter-nesting epigaeic predator** pred_ll_eg Exemplars: *Leptogenys; Platythyrea*
gp_sb_ll sp_sb_ll	pred_sb_ll	**Subterranean predator** pred_sub Exemplars: *Proceratium; Stigmatomma; Leptanilla*

Table S2.

Schematic of ecomorph syndrome collapse: ecomorphs were collapsed based on ecological and morphological overlap between groups, and qualitative assessment of likely ecological overlap (leaf litter foragers may also forage on the surface of the ground, for example). Final column shows ecomorph syndrome abbreviations, definitions, and exemplar taxa (abbreviations used in raw dataset available on Dryad (DOI: https://doi.org/10.5061/dryad.kh1893243).

Species	Specimen accession number	Caste	Sampling method
Ceratomyrmex planus	BALTJ_025	Worker	Measured under light microscopy
Ceratomyrmex ellenbergeri	BALTJ_016	Worker	Measured under light microscopy
Ceratomyrmex ellenbergeri	BALTJ_027	Worker	Measured under light microscopy
Ceratomyrmex ellenbergeri	BALTJ_029	Worker	Measured under light microscopy
Protoceratomyrmex revelatus	BALTJ_043	Worker	Measured under light microscopy
Linguamyrmex sp5	BALTJ_050	Worker	Measured under light microscopy
Linguamyrmex sp4	BALTJ_031	Worker	Measured under light microscopy
Linguamyrmex brevicornis	BALTJ_030	Worker	Measured under light microscopy
Linguamyrmex sp2	BALTJ_059	Worker	Measured under light microscopy
Linguamyrmex sp1	BALTJ_056	Worker	Measured under light microscopy
Haidomyrmex sp3	BALTJ_022	Worker	Measured under light microscopy
Haidomyrmex sp5	BALTJ_017	Worker	Measured under light microscopy
Haidomyrmex sp5	BALTJ_009	Worker	Measured under light microscopy
Haidomyrmex sp5	BALTJ_066	Worker	Measured under light microscopy
Haidomyrmex sp5	BALTJ_007	Worker	Measured under light microscopy
Haidomyrmex scimitarus	BALTJ_004	Worker	Measured under light microscopy
Haidomyrmex sp5	BALTJ_011	Worker	Measured under light microscopy
Haidomyrmex sp4	BALTJ_003	Worker	Measured under light microscopy
Haidomyrmex indet1	BALTJ_010	Worker	Measured under light microscopy
Haidomyrmex indet2	BALTJ_065	Worker	Measured under light microscopy
Linguamyrmex vladi	BuPH-1	Worker	Measured from micro-CT reconstruction
Haidomyrmex scimitarus	Bu-FB80	Dealate queen	Measured from micro-CT reconstruction
Pseudomyrmex c.f. macrops	DR-14-1021	Worker	Measured from micro-CT reconstruction
Dhagnathos autokrator	IGR.BU-003	Alate queen	Measured under light microscopy

Table S3.

List of all fossil specimens included in the study, with caste and measurement type information included. All specimens with accession numbers beginning in BALTJ are from a private collection, while specimens with alternate accession numbers are housed at the American Museum of Natural History (*Linguamyrmex vladi* and *Haidomyrmex scimitarus*); the New Jersey Institute of Technology (*Pseudomyrmex macrops*); and at the University of Rennes (*Dhagnathos autokrator*).

Species	Cn	Gr	Lg	Ll	Sb	Predicted aspect
Linguamyrmex vladi	0.0322	0.502	0.0182	0.35	0.0976	Gr
Haidomyrmex scimitarus	0.136	0.3546	0.0466	0.3012	0.1616	Gr
Pseudomyrmex macrops	0.0892	0.0846	0.7778	0.0416	0.0068	Lg
Dhagnathos autokrator	0.0424	0.6124	0.0658	0.1712	0.1082	Gr

Table S4.

Nesting niche prediction votes when using model trained on full morphometric dataset, linear trait measurements; functional morphology.

Species	Ab	CR	Eg	Ll	Predicted aspect
Linguamyrmex vladi	0.075	0.1058	0.4062	0.413	Ll
Haidomyrmex scimitarus	0.2614	0.1728	0.3334	0.2324	Eg
Pseudomyrmex macrops	0.9048	0.0074	0.0322	0.0556	Ab
Dhagnathos autokrator	0.2752	0.1276	0.43	0.1672	Eg

Table S5.

Foraging niche prediction votes when using model trained on full morphometric dataset, linear trait measurements; functional morphology.

Species	Fg	Gn	GP	Om	Py	SP	Predicted aspect
Linguamyrmex vladi	0.2072	0.1658	0.3222	0.1426	0.0072	0.155	GP
Haidomyrmex scimitarus	0.0994	0.0576	0.304	0.277	0.0062	0.2558	GP
Pseudomyrmex macrops	0.018	0	0.2766	0.2616	0.3034	0.1404	Py
Dhagnathos autokrator	0.043	0.0496	0.1808	0.232	0.0114	0.4832	SP

Table S6.

Functional role prediction votes when using model trained on full morphometric dataset, linear trait measurements; functional morphology.

Species	om_cn_ab	om_grll_eg	om_leaf	om_lg_ab	pred_cr	pred_gr_egll	pred_leaf	pred_lg_ab	pred_ll_eg	pred_sub	Predicted aspect
Linguamyrmex vladi	0.0416	0.4052	0.085	0.0102	0.0718	0.0836	0.2484	0.0122	0.0352	0.0068	om_grll_eg
Haidomyrmex scimitarus	0.096	0.338	0.015	0.01	0.0656	0.1426	0.1952	0.013	0.1214	0.0032	om_grll_eg
Pseudomyrmex macrops	0.159	0.054	0.0154	0.4104	0.0104	0.0078	0.048	0.287	6.00E-04	0.0074	om_lg_ab
Dhagnathos autokrator	0.0144	0.248	0	0.0102	0.0178	0.4646	0.1218	0.1052	0.0174	0	pred_gr_egll

Table S7.

Ecomorph prediction votes when using model trained on full morphometric dataset, linear trait measurements; functional morphology.

Species	Cn	Gr	Lg	Ll	Sb	Predicted aspect
Linguamyrmex vladi	0.0232	0.1886	0.03	0.5856	0.1726	Ll
Haidomyrmex scimitarus	0.039	0.4696	0.0574	0.2966	0.1374	Gr
Pseudomyrmex macrops	0.0924	0.084	0.7782	0.04	0.0054	Lg
Dhagnathos autokrator	0.0088	0.68	0.0474	0.1728	0.091	Gr

Table S8.

Nesting niche prediction votes when using model trained on full morphometric dataset, linear trait measurements, homologous morphology.

Species	Ab	CR	Eg	Ll	Predicted aspect
Linguamyrmex vladi	0.0528	0.158	0.3324	0.4568	Ll
Haidomyrmex scimitarus	0.2258	0.1488	0.334	0.2914	Eg
Pseudomyrmex macrops	0.9014	0.0084	0.0304	0.0598	Ab
Dhagnathos autokrator	0.2124	0.1082	0.4696	0.2098	Eg

Table S9.

Foraging niche prediction votes when using model trained on full morphometric dataset, linear trait measurements, homologous morphology.

Species	Fg	Gn	GP	Om	Py	SP	Predicted aspect
Linguamyrmex vladi	0.055	0.1854	0.3942	0.1782	0.0268	0.1604	GP
Haidomyrmex scimitarus	0.019	0.0436	0.2066	0.3202	0.0476	0.363	SP
Pseudomyrmex macrops	0.0188	2.00E-04	0.2766	0.2478	0.313	0.1436	Py
Dhagnathos autokrator	0.0248	0.0418	0.0614	0.2192	0.0254	0.6274	SP

Table S10.
Functional role prediction votes when using model trained on full morphometric dataset, linear trait measurements, homologous morphology.

Species	om_cn_ab	om_grll_eg	om_leaf	om_lg_ab	pred_cr	pred_gr_egll	pred_leaf	pred_lg_ab	pred_ll_eg	pred_sub	Predicted aspect
Linguamyrmex vladi	0.0308	0.3514	0.0834	0.0508	0.116	0.0496	0.283	0.0048	0.0244	0.0058	om_grll_eg
Haidomyrmex scimitarus	0.0216	0.3756	0.0134	0.0598	0.0558	0.112	0.2732	0.0128	0.0708	0.005	om_grll_eg
Pseudomyrmex macrops	0.1624	0.0568	0.0116	0.4136	0.0142	0.0092	0.0456	0.279	2.00E-04	0.0074	om_lg_ab
Dhagnathos autokrator	0.0048	0.2558	0	0.0328	0.0202	0.475	0.1918	0.0134	0.0052	0	pred_gr_egll

Table S11.

Ecomorph prediction votes when using model trained on full morphometric dataset, linear trait measurements, homologous morphology.

Species	Cn	Gr	Lg	Ll	Sb	Predicted aspect
Linguamyrmex vladi	0.049	0.6252	0.0074	0.2694	0.049	Gr
Haidomyrmex scimitarus	0.0266	0.5414	0.0972	0.2838	0.051	Gr
Pseudomyrmex macrops	0.0086	0.0686	0.843	0.0678	0.012	Lg
Dhagnathos autokrator	0.0184	0.4248	0.0814	0.42	0.0554	Gr

Table S12.

Nesting niche prediction votes when using model trained on full morphometric dataset; shape ratio trait measurements; functional morphology.

Species	Ab	CR	Eg	Ll	Predicted aspect
Linguamyrmex vladi	0.1572	0.062	0.6564	0.1244	Eg
Haidomyrmex scimitarus	0.2086	0.108	0.4724	0.211	Eg
Pseudomyrmex macrops	0.8186	0.0142	0.1376	0.0296	Ab
Dhagnathos autokrator	0.1462	0.067	0.3526	0.4342	Ll

Table S13.

Foraging niche prediction votes when using model trained on full morphometric dataset; shape ratio trait measurements; functional morphology.

Species	Fg	Gn	GP	Om	Py	SP	Predicted aspect
Linguamyrmex vladi	0.037	0.0328	0.3172	0.362	8.00E-04	0.2502	Om
Haidomyrmex scimitarus	0.0074	0.02	0.4008	0.1708	0.0202	0.3808	GP
Pseudomyrmex macrops	8.00E-04	0.0044	0.0866	0.051	0.7116	0.1456	Py
Dhagnathos autokrator	0.0458	0.0158	0.383	0.1612	0.0322	0.362	GP

Table S14.
Functional role prediction votes when using model trained on full morphometric dataset; shape ratio trait measurements; functional morphology.

Species	om_cn_ab	om_grll_eg	om_leaf	om_lg_ab	pred_cr	pred_gr_egll	pred_leaf	pred_lg_ab	pred_ll_eg	pred_sub	Predicted aspect
Linguamyrmex vladi	0.0684	0.2738	0.0552	6.00E-04	0.0558	0.4122	0.1088	0.0058	0.0192	2.00E-04	pred_gr_egll
Haidomyrmex scimitarus	0.0114	0.1738	0.0102	0.0146	0.0308	0.4666	0.1072	0.0624	0.1136	0.0094	pred_gr_egll
Pseudomyrmex macrops	0.0066	0.0354	0.0048	0.6404	0.0072	0.0222	0.0098	0.231	0.0406	0.002	om_lg_ab
Dhagnathos autokrator	0.0136	0.1948	0.025	0.0136	0.0216	0.2822	0.3438	0.0352	0.059	0.0112	pred_leaf

Table S15.

Ecomorph prediction votes when using model trained on full morphometric dataset; shape ratio trait measurements; functional morphology.

Species	Cn	Gr	Lg	Ll	Sb	Predicted aspect
Linguamyrmex vladi	0.0366	0.674	0.0064	0.2228	0.0602	Gr
Haidomyrmex scimitarus	0.0206	0.6094	0.0786	0.234	0.0574	Gr
Pseudomyrmex macrops	0.0138	0.0708	0.8422	0.0638	0.0094	Lg
Dhagnathos autokrator	0.0202	0.2926	0.1466	0.485	0.0556	Ll

Table S16.

Nesting niche prediction votes when using model trained on full morphometric dataset, shape ratio trait measurements; homologous morphology.

Species	Ab	CR	Eg	Ll	Predicted aspect
Linguamyrmex vladi	0.1468	0.0678	0.6546	0.1308	Eg
Haidomyrmex scimitarus	0.1956	0.1006	0.509	0.1948	Eg
Pseudomyrmex macrops	0.8224	0.0124	0.1394	0.0258	Ab
Dhagnathos autokrator	0.1982	0.062	0.261	0.4788	Ll

Table S17.

Foraging niche prediction votes when using model trained on full morphometric dataset, shape ratio trait measurements; homologous morphology.

Species	Fg	Gn	GP	Om	Py	SP	Predicted aspect
Linguamyrmex vladi	0.0276	0.0546	0.2514	0.3588	0.001	0.3066	Om
Haidomyrmex scimitarus	0.003	0.0196	0.2828	0.1952	0.037	0.4624	SP
Pseudomyrmex macrops	0	0.005	0.0872	0.0454	0.6976	0.1648	Py
Dhagnathos autokrator	0.0114	0.017	0.2314	0.1764	0.046	0.5178	SP

Table S18.

Functional role prediction votes when using model trained on full morphometric dataset, shape ratio trait measurements; homologous morphology.

Species	om_cn_ab	om_grll_eg	om_leaf	om_lg_ab	pred_cr	pred_gr_egll	pred_leaf	pred_lg_ab	pred_ll_eg	pred_sub	Predicted aspect
Linguamyrmex vladi	0.05	0.303	0.0564	2.00E-04	0.0574	0.4042	0.1094	0.0082	0.011	2.00E-04	pred_gr_egll
Haidomyrmex scimitarus	0.0058	0.2034	0.0114	0.0124	0.0298	0.5468	0.091	0.0528	0.0294	0.0172	pred_gr_egll
Pseudomyrmex macrops	0.0062	0.04	0.003	0.6426	0.0074	0.0238	0.0102	0.2282	0.0372	0.0014	om_lg_ab
Dhagnathos autokrator	0.0156	0.1462	0.0214	0.0344	0.0212	0.1492	0.4522	0.1158	0.0172	0.0268	pred_leaf

Table S19.

Ecomorph prediction votes when using model trained on full morphometric dataset, shape ratio trait measurements; homologous morphology.

Species	Cn	Gr	Lg	Ll	Sb	Predicted aspect
Linguamyrmex vladi	0.033	0.3944	0.0242	0.4636	0.0848	Ll
Haidomyrmex scimitarus	0.0164	0.3428	0.1238	0.4516	0.0654	Ll
Pseudomyrmex macrops	0.0214	0.0716	0.8258	0.0712	0.01	Lg
Dhagnathos autokrator	0.0202	0.3486	0.0812	0.488	0.062	Ll

Table S20.

Nesting niche prediction votes when using model trained on full morphometric dataset, log-shape variable measurements; functional morphology.

Species	Ab	CR	Eg	Ll	Predicted aspect
Linguamyrmex vladi	0.0954	0.0816	0.4652	0.3578	Eg
Haidomyrmex scimitarus	0.1636	0.1528	0.3204	0.3632	Ll
Pseudomyrmex macrops	0.8032	0.024	0.112	0.0608	Ab
Dhagnathos autokrator	0.1284	0.0824	0.2326	0.5566	Ll

Table S21.

Foraging niche prediction votes when using model trained on full morphometric dataset, log-shape variable measurements; functional morphology.

Species	Fg	Gn	GP	Om	Py	SP	Predicted aspect
Linguamyrmex vladi	0.0526	0.0516	0.3292	0.3226	0.0034	0.2406	GP
Haidomyrmex scimitarus	0.011	0.0138	0.4252	0.1884	0.0314	0.3302	SP
Pseudomyrmex macrops	4.00E-04	0.0042	0.0998	0.0572	0.7034	0.135	Py
Dhagnathos autokrator	0.041	0.0124	0.3924	0.1872	0.031	0.336	GP

Table S22.

Functional role prediction votes when using model trained on full morphometric dataset, log-shape variable measurements; functional morphology.

Species	om_cn_ab	om_grll_eg	om_leaf	om_lg_ab	pred_cr	pred_gr_egll	pred_leaf	pred_lg_ab	pred_ll_eg	pred_sub	Predicted aspect
Linguamyrmex vladi	0.0692	0.2434	0.1376	0.0034	0.0574	0.247	0.2016	0.0224	0.0174	6.00E-04	om_grll_eg
Haidomyrmex scimitarus	0.0158	0.184	0.0396	0.0274	0.0394	0.22	0.2782	0.096	0.0882	0.0114	pred_leaf
Pseudomyrmex macrops	0.0138	0.0518	0.0072	0.6466	0.0082	0.0104	0.025	0.2114	0.0238	0.0018	om_lg_ab
Dhagnathos autokrator	0.0198	0.1836	0.0484	0.0204	0.0262	0.157	0.4384	0.055	0.0412	0.01	pred_leaf

Table S23.

Ecomorph prediction votes when using model trained on full morphometric dataset, log-shape variable measurements; functional morphology.

Species	Cn	Gr	Lg	Ll	Sb	Predicted aspect
Linguamyrmex vladi	0.0302	0.3864	0.0254	0.4378	0.1202	Ll
Haidomyrmex scimitarus	0.0142	0.3404	0.1008	0.4436	0.101	Ll
Pseudomyrmex macrops	0.021	0.089	0.8096	0.069	0.0114	Lg
Dhagnathos autokrator	0.0194	0.1982	0.1256	0.5806	0.0762	Ll

Table S24.

Nesting niche prediction votes when using model trained on full morphometric dataset, log-shape variable measurements; homologous morphology.

Species	Ab	CR	Eg	Ll	Predicted aspect
Linguamyrmex vladi	0.0966	0.1034	0.4488	0.3512	Eg
Haidomyrmex scimitarus	0.151	0.1666	0.3178	0.3646	Ll
Pseudomyrmex macrops	0.8098	0.022	0.1072	0.061	Ab
Dhagnathos autokrator	0.1552	0.0962	0.1778	0.5708	Ll

Table S25.

Foraging niche prediction votes when using model trained on full morphometric dataset, log-shape variable measurements; homologous morphology.

Species	Fg	Gn	GP	Om	Py	SP	Predicted aspect
Linguamyrmex vladi	0.0416	0.0556	0.2538	0.346	0.0014	0.3016	Om
Haidomyrmex scimitarus	0.0058	0.018	0.3232	0.2082	0.0364	0.4084	SP
Pseudomyrmex macrops	6.00E-04	0.007	0.0938	0.0638	0.6954	0.1394	Py
Dhagnathos autokrator	0.0144	0.0166	0.2528	0.1814	0.0472	0.4876	SP

Table S26.

Functional role prediction votes when using model trained on full morphometric dataset, log-shape variable measurements; homologous morphology.

Species	om_cn_ab	om_grll_eg	om_leaf	om_lg_ab	pred_cr	pred_gr_egll	pred_leaf	pred_lg_ab	pred_ll_eg	pred_sub	Predicted aspect
Linguamyrmex vladi	0.0486	0.2668	0.1392	0.0044	0.0634	0.2518	0.1924	0.0168	0.0126	0.004	om_grll_eg
Haidomyrmex scimitarus	0.0104	0.2208	0.0362	0.0306	0.0522	0.2444	0.268	0.0764	0.0426	0.0184	pred_gr_egll
Pseudomyrmex macrops	0.0114	0.0492	0.0068	0.6548	0.0106	0.0108	0.0258	0.2054	0.024	0.0012	om_lg_ab
Dhagnathos autokrator	0.0236	0.1238	0.033	0.0284	0.025	0.0812	0.5186	0.1332	0.0132	0.02	pred_leaf

Table S27.

Ecomorph prediction votes when using model trained on full morphometric dataset, log-shape variable measurements; homologous morphology.

Species	Cn	Gr	Lg	Ll	Sb	Predicted aspect
Ceratomyrmex planus	0.0598	0.3838	0.0762	0.4338	0.0464	Ll
Ceratomyrmex ellenbergeri	0.057	0.485	0.0416	0.2394	0.177	Gr
Ceratomyrmex ellenbergeri	0.0382	0.4644	0.1014	0.3522	0.0438	Gr
Ceratomyrmex ellenbergeri	0.0736	0.519	0.0402	0.2826	0.0846	Gr
Protoceratomyrmex revelatus	0.0762	0.5304	0.0466	0.2896	0.0572	Gr
Linguamyrmex sp5	0.0912	0.6572	0.0166	0.202	0.033	Gr
Linguamyrmex sp4	0.0646	0.5374	0.0234	0.2556	0.119	Gr
Linguamyrmex brevicornis	0.0552	0.5154	0.0342	0.36	0.0352	Gr
Linguamyrmex sp2	0.0572	0.4372	0.0872	0.3666	0.0518	Gr
Linguamyrmex sp1	0.0662	0.4752	0.0368	0.2536	0.1682	Gr
Haidomyrmex sp3	0.0508	0.3036	0.2456	0.3598	0.0402	Ll
Haidomyrmex sp5	0.0426	0.355	0.1906	0.361	0.0508	Ll
Haidomyrmex sp5	0.0352	0.3664	0.2152	0.3422	0.041	Gr
Haidomyrmex sp5	0.0468	0.3816	0.1986	0.3056	0.0674	Gr
Haidomyrmex sp5	0.0376	0.3426	0.2926	0.2666	0.0606	Cn
Haidomyrmex scimitarus	0.0806	0.442	0.0288	0.249	0.1996	Gr
Haidomyrmex sp5	0.0412	0.4184	0.1834	0.2888	0.0682	Gr
Haidomyrmex sp4	0.0752	0.4584	0.0474	0.2482	0.1708	Gr
Haidomyrmex indet1	0.0294	0.3846	0.1996	0.3448	0.0416	Gr
Haidomyrmex indet2	0.0192	0.2474	0.2866	0.3914	0.0554	Ll

Table S28.

Nesting niche prediction votes when using model trained on subset of complete morphometrics dataset; linear trait measurements; functional morphology.

Species	Ab	CR	Eg	Ll	Predicted aspect
Ceratomyrmex planus	0.0986	0.0744	0.2564	0.5706	Ll
Ceratomyrmex ellenbergeri	0.1966	0.1784	0.384	0.241	Eg
Ceratomyrmex ellenbergeri	0.172	0.0578	0.2922	0.478	Ll
Ceratomyrmex ellenbergeri	0.13	0.0842	0.4284	0.3574	Eg
Protoceratomyrmex revelatus	0.1536	0.089	0.4234	0.334	Eg
Linguamyrmex sp5	0.252	0.019	0.653	0.076	Eg
Linguamyrmex sp4	0.238	0.0954	0.512	0.1546	Eg
Linguamyrmex brevicornis	0.1	0.0648	0.3994	0.4358	Ll
Linguamyrmex sp2	0.1608	0.0972	0.3546	0.3874	Ll
Linguamyrmex sp1	0.2018	0.1692	0.425	0.204	Eg
Haidomyrmex sp3	0.3014	0.0798	0.1928	0.426	Ll
Haidomyrmex sp5	0.2274	0.0466	0.2878	0.4382	Ll
Haidomyrmex sp5	0.2136	0.076	0.3052	0.4052	Ll
Haidomyrmex sp5	0.2506	0.0792	0.2868	0.3834	Ll
Haidomyrmex sp5	0.2774	0.0734	0.2738	0.3754	Ll
Haidomyrmex scimitarus	0.2156	0.1968	0.3992	0.1884	Eg
Haidomyrmex sp5	0.2306	0.1016	0.2492	0.4186	Ll
Haidomyrmex sp4	0.216	0.2006	0.4204	0.163	Eg
Haidomyrmex indet1	0.2432	0.1048	0.2476	0.4044	Ll
Haidomyrmex indet2	0.2582	0.0602	0.2704	0.4112	Ll

Table S29.

Foraging niche prediction votes when using model trained on subset of complete morphometrics dataset; linear trait measurements; functional morphology.

Species	Fg	Gn	GP	Om	Py	SP	Predicted aspect
Ceratomyrmex planus	0.1016	0.0506	0.1618	0.253	0.0566	0.3764	SP
Ceratomyrmex ellenbergeri	0.1676	0.0496	0.2944	0.2472	0.014	0.2272	GP
Ceratomyrmex ellenbergeri	0.1592	0.0742	0.3004	0.1192	0.0364	0.3106	SP
Ceratomyrmex ellenbergeri	0.2452	0.0546	0.2304	0.152	0.0104	0.3074	SP
Protoceratomyrmex revelatus	0.3096	0.08	0.0948	0.2104	0.0666	0.2386	Fg
Linguamyrmex sp5	0.1842	0.055	0.1616	0.3338	0.0028	0.2626	Om
Linguamyrmex sp4	0.1486	0.0734	0.2288	0.268	0.0068	0.2744	SP
Linguamyrmex brevicornis	0.229	0.1706	0.135	0.1818	0.0452	0.2384	SP
Linguamyrmex sp2	0.1612	0.0706	0.3864	0.161	0.0234	0.1974	GP
Linguamyrmex sp1	0.1314	0.0716	0.2904	0.2572	0.0114	0.238	GP
Haidomyrmex sp3	0.11	0.042	0.151	0.1024	0.1224	0.4722	SP
Haidomyrmex sp5	0.1528	0.047	0.2392	0.1324	0.0618	0.3668	SP
Haidomyrmex sp5	0.1302	0.0378	0.2434	0.1506	0.0624	0.3756	SP
Haidomyrmex sp5	0.1756	0.06	0.1452	0.1302	0.0696	0.4194	SP
Haidomyrmex sp5	0.2224	0.0808	0.1288	0.101	0.0666	0.4004	SP
Haidomyrmex scimitarus	0.108	0.0286	0.2866	0.3028	0.0176	0.2564	Om
Haidomyrmex sp5	0.1756	0.0372	0.187	0.1384	0.0416	0.4202	SP
Haidomyrmex sp4	0.1548	0.0384	0.275	0.278	0.0132	0.2406	Om
Haidomyrmex indet1	0.208	0.0376	0.2088	0.1938	0.0544	0.2974	SP
Haidomyrmex indet2	0.113	0.075	0.1456	0.0944	0.0948	0.4772	SP

Table S30.
Functional role prediction votes when using model trained on subset of complete morphometrics dataset; linear trait measurements; functional morphology.

Species	om_cn_ab	om_grll_eg	om_leaf	om_lg_ab	pred_cr	pred_gr_egll	pred_leaf	pred_lg_ab	pred_ll_eg	pred_sub	Predicted aspect
Ceratomyrmex planus	0.0578	0.2526	0.158	0.0544	0.0754	0.064	0.2268	0.0848	0.0038	0.0224	om_grll_eg
Ceratomyrmex ellenbergeri	0.0656	0.3268	0.0108	0.0118	0.0564	0.1744	0.2716	0.017	0.0654	0	om_grll_eg
Ceratomyrmex ellenbergeri	0.0436	0.2244	0.0762	0.0712	0.0444	0.0384	0.4158	0.0436	0.0324	0.01	pred_leaf
Ceratomyrmex ellenbergeri	0.0506	0.2992	0.0264	0.026	0.0462	0.0866	0.3874	0.012	0.0626	0.003	pred_leaf
Protoceratomyrmex revelatus	0.1194	0.405	0.108	0.0892	0.0718	0.028	0.111	0.0174	0.0446	0.0056	om_grll_eg
Linguamyrmex sp5	0.0838	0.396	0.0028	0.0014	0.012	0.2324	0.1946	0.017	0.0598	0	om_grll_eg
Linguamyrmex sp4	0.0814	0.3842	0.0034	0.0026	0.0236	0.1794	0.2432	0.0106	0.0714	0	om_grll_eg
Linguamyrmex brevicornis	0.0716	0.4046	0.2012	0.065	0.0378	0.0432	0.138	0.0076	0.0254	0.0056	om_grll_eg
Linguamyrmex sp2	0.0468	0.2786	0.0312	0.0276	0.064	0.0502	0.4588	0.0112	0.0298	0.0018	pred_leaf
Linguamyrmex sp1	0.079	0.3368	0.008	0.0062	0.043	0.2066	0.234	0.0132	0.073	0	om_grll_eg
Haidomyrmex sp3	0.1102	0.1584	0.0758	0.1518	0.0394	0.0286	0.2254	0.189	0.0086	0.0128	pred_leaf
Haidomyrmex sp5	0.0472	0.1746	0.0562	0.1264	0.0416	0.0444	0.3034	0.1356	0.0572	0.0134	pred_leaf
Haidomyrmex sp5	0.0438	0.207	0.044	0.1276	0.071	0.0358	0.2872	0.1122	0.0628	0.0086	pred_leaf
Haidomyrmex sp5	0.06	0.1958	0.0538	0.1508	0.0646	0.0372	0.2004	0.147	0.0746	0.0158	pred_leaf
Haidomyrmex sp5	0.0418	0.2396	0.0426	0.1212	0.0542	0.0428	0.209	0.1694	0.0548	0.0246	om_grll_eg

Haidomyrmex scimitarus	0.082	0.3636	0.0036	0.0108	0.0596	0.2104	0.1606	0.0096	0.0998	0	om_grll_eg
Haidomyrmex sp5	0.0688	0.2302	0.091	0.0952	0.0628	0.0496	0.176	0.1854	0.0224	0.0186	om_grll_eg
Haidomyrmex sp4	0.0898	0.3548	0.0016	0.0156	0.0662	0.2046	0.1214	0.011	0.1344	0	om_grll_eg
Haidomyrmex indet1	0.0544	0.2744	0.106	0.109	0.053	0.0436	0.1388	0.1768	0.0294	0.0146	om_grll_eg
Haidomyrmex indet2	0.0358	0.2108	0.0304	0.162	0.0486	0.0794	0.1852	0.1034	0.125	0.0194	om_grll_eg

Table S31.

Ecomorph prediction votes when using model trained on subset of complete morphometrics dataset; linear trait measurements; functional morphology.

Species	Cn	Gr	Lg	Ll	Sb	Predicted aspect
Ceratomyrmex planus	0.0384	0.2442	0.0898	0.5854	0.0422	Ll
Ceratomyrmex ellenbergeri	0.0074	0.4942	0.0608	0.2844	0.1532	Gr
Ceratomyrmex ellenbergeri	0.0574	0.1966	0.1402	0.507	0.0988	Ll
Ceratomyrmex ellenbergeri	0.034	0.2198	0.0466	0.5722	0.1274	Ll
Protoceratomyrmex revelatus	0.033	0.2098	0.0432	0.6314	0.0826	Ll
Linguamyrmex sp5	0.0084	0.8596	0.0304	0.0828	0.0188	Gr
Linguamyrmex sp4	0.0058	0.6526	0.046	0.1858	0.1098	Gr
Linguamyrmex brevicornis	0.0482	0.1406	0.0376	0.708	0.0656	Ll
Linguamyrmex sp2	0.019	0.184	0.1028	0.6352	0.059	Ll
Linguamyrmex sp1	0.0088	0.577	0.0556	0.2204	0.1382	Gr
Haidomyrmex sp3	0.0662	0.2	0.2552	0.4328	0.0458	Ll
Haidomyrmex sp5	0.043	0.3078	0.2038	0.401	0.0444	Ll
Haidomyrmex sp5	0.0374	0.1636	0.2776	0.4484	0.073	Ll
Haidomyrmex sp5	0.0424	0.1274	0.234	0.5152	0.081	Ll
Haidomyrmex sp5	0.0202	0.1118	0.2906	0.4878	0.0896	Ll
Haidomyrmex scimitarus	0.0134	0.5824	0.0606	0.214	0.1296	Gr
Haidomyrmex sp5	0.062	0.1338	0.223	0.4516	0.1296	Ll
Haidomyrmex sp4	0.0292	0.5052	0.079	0.2054	0.1812	Gr
Haidomyrmex indet1	0.0266	0.3602	0.2272	0.3438	0.0422	Gr
Haidomyrmex indet2	0.0136	0.2024	0.2682	0.446	0.0698	Ll

Table S32.

Nesting niche prediction votes when using model trained on subset of complete morphometrics dataset; linear trait measurements; homologous morphology.

Species	Ab	CR	Eg	Ll	Predicted aspect
Ceratomyrmex planus	0.0864	0.0914	0.1778	0.6444	Ll
Ceratomyrmex ellenbergeri	0.0928	0.1676	0.4108	0.3288	Eg
Ceratomyrmex ellenbergeri	0.1808	0.075	0.2518	0.4924	Ll
Ceratomyrmex ellenbergeri	0.0866	0.1364	0.3178	0.4592	Ll
Protoceratomyrmex revelatus	0.0776	0.102	0.3904	0.43	Ll
Linguamyrmex sp5	0.1526	0.0194	0.7488	0.0792	Eg
Linguamyrmex sp4	0.1634	0.1106	0.5472	0.1788	Eg
Linguamyrmex brevicornis	0.0778	0.0826	0.2944	0.5452	Ll
Linguamyrmex sp2	0.065	0.1212	0.2836	0.5302	Ll
Linguamyrmex sp1	0.1474	0.1606	0.4448	0.2472	Eg
Haidomyrmex sp3	0.3078	0.0824	0.1786	0.4312	Ll
Haidomyrmex sp5	0.217	0.0488	0.3048	0.4294	Ll
Haidomyrmex sp5	0.2186	0.0836	0.2414	0.4564	Ll
Haidomyrmex sp5	0.232	0.059	0.263	0.446	Ll
Haidomyrmex sp5	0.232	0.1114	0.2186	0.438	Ll
Haidomyrmex scimitarus	0.2052	0.13	0.414	0.2508	Eg
Haidomyrmex sp5	0.2532	0.0988	0.171	0.477	Ll
Haidomyrmex sp4	0.1976	0.1906	0.4222	0.1896	Eg
Haidomyrmex indet1	0.2514	0.085	0.2622	0.4014	Ll
Haidomyrmex indet2	0.208	0.0832	0.258	0.4508	Ll

Table S33.
Foraging niche prediction votes when using model trained on subset of complete morphometrics dataset; linear trait measurements; homologous morphology.

Species	Fg	Gn	GP	Om	Py	SP	Predicted aspect
Ceratomyrmex planus	0.0998	0.0466	0.1796	0.1574	0.0518	0.4648	SP
Ceratomyrmex ellenbergeri	0.0318	0.061	0.3106	0.2362	0.08	0.2804	GP
Ceratomyrmex ellenbergeri	0.0848	0.1064	0.322	0.1258	0.0582	0.3028	GP
Ceratomyrmex ellenbergeri	0.046	0.0978	0.3204	0.2192	0.037	0.2796	GP
Protoceratomyrmex revelatus	0.0794	0.0954	0.216	0.289	0.067	0.2532	Om
Linguamyrmex sp5	0.0396	0.0306	0.1186	0.4328	0.0542	0.3242	Om
Linguamyrmex sp4	0.0216	0.0636	0.1878	0.3358	0.0732	0.318	Om
Linguamyrmex brevicornis	0.0844	0.1938	0.194	0.2334	0.0452	0.2492	SP
Linguamyrmex sp2	0.0386	0.1178	0.3982	0.1722	0.0582	0.215	GP
Linguamyrmex sp1	0.0234	0.055	0.2526	0.3058	0.081	0.2822	Om
Haidomyrmex sp3	0.057	0.0388	0.1812	0.1338	0.1736	0.4156	SP
Haidomyrmex sp5	0.1042	0.0644	0.2236	0.1662	0.0912	0.3504	SP
Haidomyrmex sp5	0.0878	0.0904	0.2576	0.1102	0.1004	0.3536	SP
Haidomyrmex sp5	0.0544	0.0852	0.195	0.1636	0.0974	0.4044	SP
Haidomyrmex sp5	0.0322	0.0854	0.2618	0.1664	0.085	0.3692	SP
Haidomyrmex scimitarus	0.0564	0.0386	0.1404	0.3496	0.0724	0.3426	SP
Haidomyrmex sp5	0.0554	0.0408	0.2708	0.1428	0.0882	0.402	SP
Haidomyrmex sp4	0.044	0.0378	0.1976	0.3738	0.0844	0.2624	Om
Haidomyrmex indet1	0.1206	0.0274	0.2576	0.1944	0.1068	0.2932	SP

Haidomyrmex indet2	0.0356	0.113	0.2284	0.1366	0.0994	0.387	SP

Table S34.

Functional role prediction votes when using model trained on subset of complete morphometrics dataset; linear trait measurements; homologous morphology.

Species	om_cn_ab	om_grll_eg	om_leaf	om_lg_ab	pred_cr	pred_gr_egll	pred_leaf	pred_lg_ab	pred_ll_eg	pred_sub	Predicted aspect
Ceratomyrmex planus	0.0424	0.135	0.219	0.0462	0.0718	0.1054	0.2652	0.093	0.0024	0.0196	pred_leaf
Ceratomyrmex ellenbergeri	0.0082	0.2986	0.0144	0.0644	0.0508	0.1856	0.3356	0.0094	0.0322	0	pred_leaf
Ceratomyrmex ellenbergeri	0.0492	0.1868	0.0918	0.0972	0.0586	0.0274	0.4056	0.0386	0.0272	0.0176	pred_leaf
Ceratomyrmex ellenbergeri	0.0366	0.2668	0.0392	0.052	0.0848	0.0512	0.409	0.0092	0.0462	0.005	pred_leaf
Protoceratomyrmex revelatus	0.0812	0.4286	0.0738	0.0708	0.105	0.0378	0.1346	0.0224	0.0384	0.0074	om_grll_eg
Linguamyrmex sp5	0.0114	0.4306	0.0036	0.0464	0.016	0.2274	0.224	0.0142	0.026	0	om_grll_eg
Linguamyrmex sp4	0.0122	0.3858	0.0062	0.051	0.0414	0.1664	0.2982	0.0082	0.0302	0	om_grll_eg
Linguamyrmex brevicornis	0.0688	0.373	0.1954	0.0668	0.0672	0.0338	0.1634	0.0052	0.0162	0.0102	om_grll_eg
Linguamyrmex sp2	0.019	0.1966	0.0568	0.065	0.089	0.0274	0.517	0.0056	0.0182	0.0054	pred_leaf
Linguamyrmex sp1	0.0102	0.3314	0.0094	0.0618	0.0484	0.199	0.295	0.011	0.0332	0	om_grll_eg
Haidomyrmex sp3	0.1096	0.167	0.0658	0.1542	0.0406	0.0172	0.2366	0.1888	0.0072	0.013	pred_leaf
Haidomyrmex sp5	0.0464	0.212	0.0738	0.1242	0.0378	0.0362	0.2596	0.1398	0.0498	0.0204	pred_leaf

Haidomyrmex sp5	0.0406	0.163	0.0836	0.1436	0.0832	0.0212	0.2748	0.1196	0.0544	0.016	pred_leaf
Haidomyrmex sp5	0.057	0.2198	0.0486	0.1436	0.0682	0.0162	0.2008	0.1536	0.067	0.0252	om_grll_eg
Haidomyrmex sp5	0.0332	0.19	0.044	0.1394	0.1132	0.014	0.2506	0.1464	0.0426	0.0266	pred_leaf
Haidomyrmex scimitarus	0.0154	0.3938	0.008	0.0652	0.0406	0.2328	0.1854	0.009	0.0492	0	om_grll_eg
Haidomyrmex sp5	0.0706	0.1688	0.0652	0.1158	0.0928	0.0496	0.198	0.1944	0.0238	0.021	pred_leaf
Haidomyrmex sp4	0.0254	0.4188	0.0042	0.0784	0.0728	0.1626	0.163	0.011	0.0628	0.001	om_grll_eg
Haidomyrmex indet1	0.043	0.2726	0.0744	0.1262	0.0422	0.0516	0.1436	0.213	0.022	0.0114	om_grll_eg
Haidomyrmex indet2	0.0324	0.1804	0.0488	0.1762	0.1038	0.0574	0.1936	0.0774	0.1062	0.0238	pred_leaf

Table S35.
Ecomorph prediction votes when using model trained on subset of complete morphometrics dataset; linear trait measurements; homologous morphology.

Species	Cn	Gr	Lg	Ll	Sb	Predicted aspect
Ceratomyrmex planus	0.0684	0.6814	0.0074	0.2158	0.027	Gr
Ceratomyrmex ellenbergeri	0.0424	0.7562	6.00E-04	0.1998	0.001	Gr
Ceratomyrmex ellenbergeri	0.0482	0.704	0.0018	0.2322	0.0138	Gr
Ceratomyrmex ellenbergeri	0.0326	0.7176	0.023	0.2146	0.0122	Gr
Protoceratomyrmex revelatus	0.0256	0.6942	0.0226	0.242	0.0156	Gr
Linguamyrmex sp5	0.0252	0.6544	0.002	0.3162	0.0022	Gr
Linguamyrmex sp4	0.0212	0.6548	0.0044	0.3188	0	Gr
Linguamyrmex brevicornis	0.2636	0.2216	0.0608	0.4474	0.0066	Ll
Linguamyrmex sp2	0.0634	0.6044	0.0108	0.3094	0.012	Gr
Linguamyrmex sp1	0.0434	0.7008	0.0024	0.239	0.0144	Gr
Haidomyrmex sp3	0.0206	0.1626	0.5006	0.2918	0.0244	Lg
Haidomyrmex sp5	0.004	0.548	0.0458	0.4	0.0022	Gr
Haidomyrmex sp5	0.0116	0.8092	0.0194	0.1556	0.0042	Gr
Haidomyrmex sp5	0.0022	0.743	0.0856	0.1658	0.0034	Gr
Haidomyrmex sp5	0.0304	0.3702	0.258	0.32	0.0214	Gr
Haidomyrmex scimitarus	0.055	0.7134	0.0088	0.2052	0.0176	Gr
Haidomyrmex sp5	0.0026	0.5238	0.2264	0.2288	0.0184	Gr
Haidomyrmex sp4	0.0066	0.707	0.0744	0.2032	0.0088	Gr

Haidomyrmex indet1	0.0022	0.7738	0.0692	0.1506	0.0042	Gr
Haidomyrmex indet2	0.003	0.5718	0.1326	0.2886	0.004	Gr

Table S36.

Nesting niche prediction votes when using model trained on subset of complete morphometrics dataset; shape ratio trait measurements; functional morphology.

Species	Ab	CR	Eg	Ll	Predicted aspect
Ceratomyrmex planus	0.1752	0.0844	0.5354	0.205	Eg
Ceratomyrmex ellenbergeri	0.1584	0.0032	0.59	0.2484	Eg
Ceratomyrmex ellenbergeri	0.1658	0.0132	0.5646	0.2564	Eg
Ceratomyrmex ellenbergeri	0.11	0.0826	0.5422	0.2652	Eg
Protoceratomyrmex revelatus	0.2024	0.0676	0.6052	0.1248	Eg
Linguamyrmex sp5	0.1838	0.0022	0.4504	0.3636	Eg
Linguamyrmex sp4	0.1978	0.002	0.5542	0.246	Eg
Linguamyrmex brevicornis	0.403	0.0424	0.2646	0.29	Ab
Linguamyrmex sp2	0.2446	0.0182	0.502	0.2352	Eg
Linguamyrmex sp1	0.2264	0.0142	0.4928	0.2666	Eg
Haidomyrmex sp3	0.3572	0.2008	0.2432	0.1988	Ab
Haidomyrmex sp5	0.1086	0.0674	0.5246	0.2994	Eg
Haidomyrmex sp5	0.1166	0.0642	0.6328	0.1864	Eg
Haidomyrmex sp5	0.1594	0.0844	0.5338	0.2224	Eg
Haidomyrmex sp5	0.2292	0.162	0.4284	0.1804	Eg
Haidomyrmex scimitarus	0.165	0.0598	0.5762	0.199	Eg
Haidomyrmex sp5	0.1918	0.0992	0.4758	0.2332	Eg

Haidomyrmex sp4	0.1104	0.0872	0.584	0.2184	Eg
Haidomyrmex indet1	0.0934	0.057	0.6406	0.209	Eg
Haidomyrmex indet2	0.1078	0.0872	0.5662	0.2388	Eg

Table S37.

Foraging niche prediction votes when using model trained on subset of complete morphometrics dataset; shape ratio trait measurements; functional morphology.

Species	Fg	Gn	GP	Om	Py	SP	Predicted aspect
Ceratomyrmex planus	0.0434	0.1026	0.1652	0.4172	2.00E-04	0.2714	Om
Ceratomyrmex ellenbergeri	0.1128	0.0178	0.5196	0.2742	0	0.075	GP
Ceratomyrmex ellenbergeri	0.0924	0.0332	0.4498	0.283	0.001	0.1406	GP
Ceratomyrmex ellenbergeri	0.066	0.0764	0.4536	0.2248	0.0022	0.177	GP
Protoceratomyrmex revelatus	0.0106	0.0128	0.1504	0.2706	0.001	0.5546	SP
Linguamyrmex sp5	0.0942	0.0364	0.3288	0.4298	0	0.1106	Om
Linguamyrmex sp4	0.0596	0.0104	0.2864	0.4004	0	0.243	Om
Linguamyrmex brevicornis	0.0314	0.024	0.1766	0.3368	0.0014	0.4298	SP
Linguamyrmex sp2	0.1124	0.0122	0.336	0.34	0	0.1994	Om
Linguamyrmex sp1	0.0606	0.0218	0.4288	0.331	0	0.1578	GP
Haidomyrmex sp3	0.009	8.00E-04	0.3848	0.101	0.0618	0.4426	SP
Haidomyrmex sp5	0.0032	0.0014	0.6024	0.1608	0.0156	0.2166	GP
Haidomyrmex sp5	0.0036	2.00E-04	0.7118	0.1194	0.0092	0.1558	GP
Haidomyrmex sp5	0.0038	0.0296	0.5182	0.1168	0.0202	0.3114	GP
Haidomyrmex sp5	0.0934	0.0184	0.4184	0.1162	0.0288	0.3248	GP
Haidomyrmex scimitarus	0.0352	0.0128	0.428	0.2884	0.0012	0.2344	GP

Haidomyrmex sp5	0.0064	0.0106	0.3556	0.094	0.0446	0.4888	SP
Haidomyrmex sp4	0.003	0.035	0.522	0.1148	0.0182	0.307	GP
Haidomyrmex indet1	0.002	0.0092	0.6058	0.0974	0.0182	0.2674	GP
Haidomyrmex indet2	0.0038	0.0374	0.2948	0.1204	0.0324	0.5112	SP

Table S38.

Functional role prediction votes when using model trained on subset of complete morphometrics dataset; shape ratio trait measurements; functional morphology.

Species	om_cn_ab	om_grll_eg	om_leaf	om_lg_ab	pred_cr	pred_gr_egll	pred_leaf	pred_lg_ab	pred_ll_eg	pred_sub	Predicted aspect
Ceratomyrmex planus	0.055	0.328	0.1102	0	0.0292	0.3218	0.1372	0.0062	0.0116	0	om_grll_eg
Ceratomyrmex ellenbergeri	0.063	0.2064	0.0466	0	0.0028	0.5138	0.1148	0	0.0522	0	pred_gr_egll
Ceratomyrmex ellenbergeri	0.059	0.216	0.0606	0	0.0142	0.3868	0.2192	0.001	0.0428	0	pred_gr_egll
Ceratomyrmex ellenbergeri	0.02	0.2284	0.0272	0.0028	0.02	0.549	0.1062	0.009	0.0364	0.001	pred_gr_egll
Protoceratomyrmex revelatus	0.0142	0.2096	0.004	0.0026	0.0146	0.5278	0.0854	0.0326	0.1084	0	pred_gr_egll
Linguamyrmex sp5	0.0452	0.3486	0.061	0	0.0012	0.238	0.272	0.0036	0.0304	0	om_grll_eg
Linguamyrmex sp4	0.0426	0.2928	0.0306	0	0.001	0.32	0.2546	0.0018	0.0566	0	pred_gr_egll
Linguamyrmex brevicornis	0.1488	0.1564	0.0172	0.0018	0.0196	0.2324	0.3284	0.0674	0.0274	0	pred_leaf
Linguamyrmex sp2	0.0688	0.2716	0.032	0	0.0136	0.3018	0.2594	0.0064	0.0456	0	pred_gr_egll
Linguamyrmex sp1	0.0508	0.2064	0.0326	0	0.011	0.3674	0.283	0.001	0.0472	0	pred_gr_egll
Haidomyrmex sp3	0.0154	0.0296	0.001	0.088	0.024	0.147	0.1572	0.4262	0.1048	0.0068	pred_lg_ab

Haidomyrmex sp5	0.0038	0.1488	0.0034	0.0074	0.0046	0.5314	0.1946	0.0162	0.0892	0	pred_gr_egll
Haidomyrmex sp5	0.0078	0.0982	0.0012	0.003	0.006	0.6876	0.0702	0.0122	0.1134	0	pred_gr_egll
Haidomyrmex sp5	0.0016	0.1446	0.002	0.0246	0.0076	0.5886	0.1084	0.044	0.0768	0.0018	pred_gr_egll
Haidomyrmex sp5	0.0298	0.111	0.0222	0.0962	0.0434	0.2588	0.1262	0.1654	0.141	0.006	pred_gr_egll
Haidomyrmex scimitarus	0.0334	0.1938	0.0172	0.0014	0.02	0.4756	0.208	0.0042	0.046	0	pred_gr_egll
Haidomyrmex sp5	0.002	0.0712	0	0.1434	0.0086	0.3544	0.1126	0.1754	0.1244	0.008	pred_gr_egll
Haidomyrmex sp4	0.0062	0.1108	0.001	0.0096	0.022	0.6138	0.0988	0.0278	0.109	0.001	pred_gr_egll
Haidomyrmex indet1	0.0014	0.084	0	0.0096	0.0118	0.7518	0.084	0.0246	0.0304	0.0022	pred_gr_egll
Haidomyrmex indet2	0.002	0.095	0.0036	0.0882	0.0156	0.431	0.1304	0.1152	0.1168	0.0022	pred_gr_egll

Table S39.

Ecomorph prediction votes when using model trained on subset of complete morphometrics dataset; shape ratio trait measurements; functional morphology.

Species	Cn	Gr	Lg	Ll	Sb	Predicted aspect
Ceratomyrmex planus	0.0392	0.5364	0.0298	0.3762	0.0184	Gr
Ceratomyrmex ellenbergeri	0.0236	0.8092	0.0024	0.1628	0.002	Gr
Ceratomyrmex ellenbergeri	0.024	0.7864	0.0026	0.176	0.011	Gr
Ceratomyrmex ellenbergeri	0.0238	0.6812	0.0424	0.2208	0.0318	Gr
Protoceratomyrmex revelatus	0.0202	0.7678	0.0176	0.1806	0.0138	Gr
Linguamyrmex sp5	0.0102	0.7622	0.002	0.2246	0.001	Gr
Linguamyrmex sp4	0.0062	0.7626	0.0038	0.2252	0.0022	Gr
Linguamyrmex brevicornis	0.2566	0.2498	0.0588	0.4286	0.0062	Ll
Linguamyrmex sp2	0.048	0.6416	0.0176	0.2768	0.016	Gr
Linguamyrmex sp1	0.0272	0.7662	0.0028	0.187	0.0168	Gr
Haidomyrmex sp3	0.013	0.1366	0.5272	0.2864	0.0368	Lg
Haidomyrmex sp5	0.0052	0.4744	0.0716	0.4432	0.0056	Gr
Haidomyrmex sp5	0.0084	0.7316	0.0324	0.2228	0.0048	Gr
Haidomyrmex sp5	0.004	0.655	0.1158	0.202	0.0232	Gr
Haidomyrmex sp5	0.0328	0.2728	0.3176	0.341	0.0358	Ll
Haidomyrmex scimitarus	0.0308	0.7934	0.01	0.1502	0.0156	Gr
Haidomyrmex sp5	0.0024	0.4766	0.2318	0.2524	0.0368	Gr

Haidomyrmex sp4	0.008	0.6384	0.094	0.2388	0.0208	Gr
Haidomyrmex indet1	0.0034	0.6742	0.0928	0.2118	0.0178	Gr
Haidomyrmex indet2	0.0022	0.5782	0.149	0.2532	0.0174	Gr

Table S40.

Nesting niche prediction votes when using model trained on subset of complete morphometrics dataset; shape ratio trait measurements; homologous morphology.

Species	Ab	CR	Eg	Ll	Predicted aspect
Ceratomyrmex planus	0.099	0.0394	0.5154	0.3462	Eg
Ceratomyrmex ellenbergeri	0.151	0.004	0.6054	0.2396	Eg
Ceratomyrmex ellenbergeri	0.0936	0.01	0.6584	0.238	Eg
Ceratomyrmex ellenbergeri	0.1374	0.0996	0.5312	0.2318	Eg
Protoceratomyrmex revelatus	0.1694	0.0638	0.6568	0.11	Eg
Linguamyrmex sp5	0.1136	0.0012	0.5652	0.32	Eg
Linguamyrmex sp4	0.1068	0.0036	0.6584	0.2312	Eg
Linguamyrmex brevicornis	0.3652	0.0286	0.3038	0.3024	Ab
Linguamyrmex sp2	0.177	0.0234	0.5522	0.2474	Eg
Linguamyrmex sp1	0.2352	0.014	0.5354	0.2154	Eg
Haidomyrmex sp3	0.4392	0.183	0.1976	0.1802	Ab
Haidomyrmex sp5	0.1836	0.0676	0.4668	0.282	Eg
Haidomyrmex sp5	0.1196	0.0638	0.611	0.2056	Eg
Haidomyrmex sp5	0.2378	0.079	0.4984	0.1848	Eg
Haidomyrmex sp5	0.31	0.2054	0.3108	0.1738	Eg
Haidomyrmex scimitarus	0.0926	0.0464	0.6744	0.1866	Eg

Haidomyrmex sp5	0.2252	0.0598	0.4966	0.2184	Eg
Haidomyrmex sp4	0.1356	0.0852	0.5698	0.2094	Eg
Haidomyrmex indet1	0.1418	0.0776	0.5776	0.203	Eg
Haidomyrmex indet2	0.1302	0.0806	0.5828	0.2064	Eg

Table S41.

Foraging niche prediction votes when using model trained on subset of complete morphometrics dataset; shape ratio trait measurements; homologous morphology.

Species	Fg	Gn	GP	Om	Py	SP	Predicted aspect
Ceratomyrmex planus	0.0398	0.1744	0.1106	0.2534	0.0066	0.4152	SP
Ceratomyrmex ellenbergeri	0.036	0.0692	0.2244	0.432	0.0066	0.2318	Om
Ceratomyrmex ellenbergeri	0.035	0.0788	0.2684	0.32	0	0.2976	Om
Ceratomyrmex ellenbergeri	0.0192	0.1224	0.1888	0.3344	0.0098	0.3254	Om
Protoceratomyrmex revelatus	0.0102	0.0098	0.1038	0.3094	0.0104	0.5564	SP
Linguamyrmex sp5	0.0436	0.0836	0.2366	0.4418	0.0068	0.1876	Om
Linguamyrmex sp4	0.0288	0.0316	0.1772	0.3616	0.0072	0.3936	SP
Linguamyrmex brevicornis	0.0306	0.0304	0.1222	0.2642	0.0108	0.5418	SP
Linguamyrmex sp2	0.0474	0.0388	0.194	0.322	0.0074	0.3904	SP
Linguamyrmex sp1	0.0226	0.0386	0.236	0.4348	0.0076	0.2604	Om
Haidomyrmex sp3	0.0024	0.001	0.2646	0.1186	0.0788	0.5346	SP
Haidomyrmex sp5	0.0018	0.0062	0.3228	0.295	0.0144	0.3598	SP
Haidomyrmex sp5	0.0026	0.0036	0.3648	0.233	0.0166	0.3794	SP
Haidomyrmex sp5	0	0.0362	0.2278	0.2348	0.0382	0.4622	SP
Haidomyrmex sp5	0.0178	0.0274	0.2834	0.1914	0.0402	0.4398	SP

Haidomyrmex scimitarus	0.0136	0.0302	0.2974	0.316	0.0084	0.3344	SP
Haidomyrmex sp5	0	0.0166	0.1994	0.091	0.075	0.618	SP
Haidomyrmex sp4	0.0024	0.0464	0.2456	0.1742	0.054	0.4774	SP
Haidomyrmex indet1	0	0.0136	0.3086	0.2266	0.0214	0.4292	SP
Haidomyrmex indet2	0.003	0.044	0.195	0.139	0.0464	0.5726	SP

Table S42.

Functional role prediction votes when using model trained on subset of complete morphometrics dataset; shape ratio trait measurements; homologous morphology.

Species	om_cn_ab	om_grll_eg	om_leaf	om_lg_ab	pred_cr	pred_gr_egll	pred_leaf	pred_lg_ab	pred_ll_eg	pred_sub	Predicted aspect
Ceratomyrmex planus	0.0384	0.2122	0.167	0.0048	0.0156	0.3348	0.1734	0.037	0.0086	0.0082	pred_gr_egll
Ceratomyrmex ellenbergeri	0.065	0.33	0.0928	0	0.0118	0.3258	0.159	0.0016	0.013	0	om_grll_eg
Ceratomyrmex ellenbergeri	0.042	0.275	0.0918	0	0.0188	0.4	0.1646	0.0022	0.005	0	pred_gr_egll
Ceratomyrmex ellenbergeri	0.0268	0.3134	0.0682	0.005	0.0436	0.3316	0.1656	0.018	0.0242	0.0036	pred_gr_egll
Protoceratomyrmex revelatus	0.0134	0.2224	0.003	0.003	0.012	0.5712	0.053	0.0196	0.102	0	pred_gr_egll
Linguamyrmex sp5	0.0264	0.3414	0.0824	0	0.004	0.2906	0.2442	0.0048	0.0058	0	om_grll_eg
Linguamyrmex sp4	0.021	0.3078	0.0362	0	0.0074	0.387	0.2282	0.0038	0.0078	0	pred_gr_egll
Linguamyrmex brevicornis	0.1364	0.1412	0.02	0.0016	0.0154	0.2688	0.3134	0.0702	0.0324	0	pred_leaf
Linguamyrmex sp2	0.0464	0.2742	0.0396	0.0012	0.0262	0.344	0.2514	0.01	0.0064	0	pred_gr_egll
Linguamyrmex sp1	0.0456	0.312	0.0502	0.0016	0.021	0.338	0.2114	0.0028	0.0172	0	pred_gr_egll

Haidomyrmex sp3	0.0076	0.0364	0	0.0766	0.0324	0.1066	0.1654	0.5032	0.0552	0.0158	pred_lg_ab
Haidomyrmex sp5	0.0122	0.2678	0.0028	0.0114	0.0102	0.3234	0.2796	0.0332	0.0586	0	pred_gr_egll
Haidomyrmex sp5	0.0046	0.209	0.0018	0.0068	0.013	0.5734	0.1688	0.0108	0.0102	0.0016	pred_gr_egll
Haidomyrmex sp5	0.008	0.2518	0	0.0352	0.02	0.3826	0.1464	0.0668	0.082	0.0068	pred_gr_egll
Haidomyrmex sp5	0.0284	0.1194	0.0216	0.0964	0.0712	0.1498	0.1526	0.2766	0.072	0.012	pred_lg_ab
Haidomyrmex scimitarus	0.0258	0.2276	0.0248	0.002	0.0206	0.5198	0.1688	0.0052	0.005	0	pred_gr_egll
Haidomyrmex sp5	0	0.0894	0	0.122	0.0102	0.3502	0.104	0.1666	0.1328	0.0236	pred_gr_egll
Haidomyrmex sp4	0.0102	0.1858	0.0022	0.016	0.0342	0.4946	0.1404	0.0396	0.0736	0.0034	pred_gr_egll
Haidomyrmex indet1	0.0036	0.2082	0	0.018	0.0268	0.5342	0.1424	0.0396	0.0224	0.0044	pred_gr_egll
Haidomyrmex indet2	0	0.1146	0.0048	0.0846	0.0274	0.426	0.1068	0.148	0.081	0.006	pred_gr_egll

Table S43.
Ecomorph prediction votes when using model trained on subset of complete morphometrics dataset; shape ratio trait measurements; homologous morphology.

Species	Cn	Gr	Lg	Ll	Sb	Predicted aspect
Ceratomyrmex planus	0.0934	0.4272	0.0378	0.3904	0.0512	Gr
Ceratomyrmex ellenbergeri	0.099	0.506	0.0084	0.3752	0.0114	Gr
Ceratomyrmex ellenbergeri	0.0666	0.4758	0.0116	0.428	0.018	Gr
Ceratomyrmex ellenbergeri	0.058	0.5162	0.0504	0.3572	0.0182	Gr
Protoceratomyrmex revelatus	0.0644	0.3684	0.0812	0.4566	0.0294	Ll
Linguamyrmex sp5	0.0324	0.4826	0.006	0.4702	0.0088	Gr
Linguamyrmex sp4	0.0366	0.4748	0.0128	0.4688	0.007	Gr
Linguamyrmex brevicornis	0.1668	0.1614	0.0912	0.5662	0.0144	Ll
Linguamyrmex sp2	0.0764	0.466	0.0174	0.4264	0.0138	Gr
Linguamyrmex sp1	0.0572	0.4728	0.0146	0.438	0.0174	Gr
Haidomyrmex sp3	0.019	0.17	0.4544	0.323	0.0336	Lg
Haidomyrmex sp5	0.024	0.4822	0.0516	0.4348	0.0074	Gr
Haidomyrmex sp5	0.0362	0.4968	0.0372	0.4196	0.0102	Gr
Haidomyrmex sp5	0.0224	0.4752	0.1224	0.3714	0.0086	Gr
Haidomyrmex sp5	0.0388	0.2972	0.2782	0.3556	0.0302	Ll
Haidomyrmex scimitarus	0.063	0.4644	0.0406	0.4016	0.0304	Gr
Haidomyrmex sp5	0.0114	0.4092	0.2424	0.3072	0.0298	Gr

Haidomyrmex sp4	0.0294	0.462	0.1	0.397	0.0116	Gr
Haidomyrmex indet1	0.0254	0.4692	0.0872	0.4104	0.0078	Gr
Haidomyrmex indet2	0.0196	0.414	0.1536	0.4066	0.0062	Gr

Table S44.

Nesting niche prediction votes when using model trained on subset of complete morphometrics dataset, log-shape variable measurements; functional morphology.

Species	Ab	CR	Eg	Ll	Predicted aspect
Ceratomyrmex planus	0.1734	0.0744	0.2814	0.4708	Ll
Ceratomyrmex ellenbergeri	0.1654	0.018	0.3412	0.4754	Ll
Ceratomyrmex ellenbergeri	0.1154	0.0274	0.371	0.4862	Ll
Ceratomyrmex ellenbergeri	0.1242	0.0908	0.3442	0.4408	Ll
Protoceratomyrmex revelatus	0.1476	0.0512	0.3506	0.4506	Ll
Linguamyrmex sp5	0.055	0.012	0.33	0.603	Ll
Linguamyrmex sp4	0.08	0.0168	0.3772	0.526	Ll
Linguamyrmex brevicornis	0.2284	0.0568	0.1408	0.574	Ll
Linguamyrmex sp2	0.1228	0.038	0.3622	0.477	Ll
Linguamyrmex sp1	0.1184	0.0254	0.3564	0.4998	Ll
Haidomyrmex sp3	0.3172	0.2226	0.1234	0.3368	Ll
Haidomyrmex sp5	0.1	0.0884	0.3318	0.4798	Ll
Haidomyrmex sp5	0.1158	0.0856	0.366	0.4326	Ll
Haidomyrmex sp5	0.1338	0.1186	0.2666	0.481	Ll
Haidomyrmex sp5	0.2274	0.1792	0.2126	0.3808	Ll
Haidomyrmex scimitarus	0.1154	0.0564	0.3712	0.457	Ll
Haidomyrmex sp5	0.1728	0.1386	0.2284	0.4602	Ll

Haidomyrmex sp4	0.1216	0.1048	0.33	0.4436	Ll
Haidomyrmex indet1	0.1166	0.0936	0.3088	0.481	Ll
Haidomyrmex indet2	0.1326	0.1128	0.3008	0.4538	Ll

Table S45.

Foraging niche prediction votes when using model trained on subset of complete morphometrics dataset, log-shape variable measurements; functional morphology.

Species	Fg	Gn	GP	Om	Py	SP	Predicted aspect
Ceratomyrmex planus	0.048	0.1128	0.1886	0.3946	0	0.256	Om
Ceratomyrmex ellenbergeri	0.132	0.0242	0.4678	0.2874	0.001	0.0876	GP
Ceratomyrmex ellenbergeri	0.089	0.0388	0.4276	0.3064	0.001	0.1372	GP
Ceratomyrmex ellenbergeri	0.09	0.0678	0.4188	0.2426	0.0026	0.1782	GP
Protoceratomyrmex revelatus	0.0176	0.017	0.1616	0.3042	0.0022	0.4974	SP
Linguamyrmex sp5	0.0878	0.0592	0.318	0.423	2.00E-04	0.1118	Om
Linguamyrmex sp4	0.0688	0.0196	0.2792	0.4124	8.00E-04	0.2192	Om
Linguamyrmex brevicornis	0.037	0.0358	0.1808	0.3312	0.002	0.4132	SP
Linguamyrmex sp2	0.1198	0.0192	0.3082	0.3652	0.001	0.1866	Om
Linguamyrmex sp1	0.0666	0.0274	0.3956	0.3476	0.0014	0.1614	GP
Haidomyrmex sp3	0.012	0.0012	0.4136	0.1192	0.0708	0.3832	GP
Haidomyrmex sp5	0.0158	0.0018	0.5512	0.2036	0.0124	0.2152	GP
Haidomyrmex sp5	0.02	0.001	0.6432	0.1574	0.0078	0.1706	GP
Haidomyrmex sp5	0.0088	0.0244	0.5178	0.1464	0.029	0.2736	GP
Haidomyrmex sp5	0.0942	0.0186	0.4072	0.1458	0.0346	0.2996	GP
Haidomyrmex scimitarus	0.0326	0.0216	0.428	0.2988	0.0028	0.2162	GP

Haidomyrmex sp5	0.009	0.0102	0.409	0.1138	0.0532	0.4048	GP
Haidomyrmex sp4	0.0114	0.0294	0.5126	0.148	0.0192	0.2794	GP
Haidomyrmex indet1	0.0094	0.0112	0.5726	0.1398	0.0168	0.2502	GP
Haidomyrmex indet2	0.0046	0.0336	0.342	0.1354	0.0408	0.4436	SP

Table S46.

Functional role prediction votes when using model trained on subset of complete morphometrics dataset, log-shape variable measurements; functional morphology.

Species	om_cn_ab	om_grll_eg	om_leaf	om_lg_ab	pred_cr	pred_gr_egll	pred_leaf	pred_lg_ab	pred_ll_eg	pred_sub	Predicted aspect
Ceratomyrmex planus	0.0888	0.321	0.1506	6.00E-04	0.0296	0.1382	0.2322	0.03	0.0088	2.00E-04	om_grll_eg
Ceratomyrmex ellenbergeri	0.0802	0.261	0.101	0.0032	0.0124	0.2796	0.198	0.0098	0.0548	0	pred_gr_egll
Ceratomyrmex ellenbergeri	0.0906	0.2436	0.1262	6.00E-04	0.017	0.1904	0.2918	0.0128	0.027	0	pred_leaf
Ceratomyrmex ellenbergeri	0.048	0.2664	0.0708	0.0114	0.0268	0.2836	0.2234	0.032	0.0376	0	pred_gr_egll
Protoceratomyrmex revelatus	0.049	0.2998	0.0296	0.0046	0.0182	0.1426	0.3026	0.0886	0.0646	4.00E-04	pred_leaf
Linguamyrmex sp5	0.068	0.2888	0.153	0	0.0044	0.131	0.3354	0.0064	0.013	0	pred_leaf
Linguamyrmex sp4	0.0674	0.2842	0.1184	4.00E-04	0.006	0.1452	0.3466	0.0118	0.0198	2.00E-04	pred_leaf
Linguamyrmex brevicornis	0.1492	0.1262	0.0452	0.0024	0.0164	0.065	0.483	0.0832	0.0292	2.00E-04	pred_leaf
Linguamyrmex sp2	0.0918	0.2704	0.1052	8.00E-04	0.0198	0.1434	0.3318	0.0182	0.0184	2.00E-04	pred_leaf
Linguamyrmex sp1	0.0832	0.2314	0.097	0.001	0.0162	0.1732	0.3564	0.0144	0.0272	0	pred_leaf
Haidomyrmex sp3	0.0166	0.0496	0.0042	0.1486	0.0178	0.0474	0.2848	0.383	0.0428	0.0052	pred_lg_ab

Haidomyrmex sp5	0.02	0.222	0.0248	0.015	0.014	0.2062	0.3946	0.0338	0.0694	2.00E-04	pred_leaf
Haidomyrmex sp5	0.0218	0.2072	0.0234	0.0104	0.0168	0.2662	0.3408	0.0362	0.0772	0	pred_leaf
Haidomyrmex sp5	0.0152	0.1692	0.0192	0.0602	0.0154	0.2122	0.3526	0.0756	0.0794	0.001	pred_leaf
Haidomyrmex sp5	0.0362	0.1434	0.0474	0.1438	0.0336	0.0942	0.2466	0.1788	0.0718	0.0042	pred_leaf
Haidomyrmex scimitarus	0.0664	0.223	0.0804	0.0032	0.024	0.216	0.3364	0.0248	0.0256	2.00E-04	pred_leaf
Haidomyrmex sp5	0.0062	0.0916	0.0042	0.219	0.0094	0.114	0.2782	0.1802	0.0864	0.0108	pred_leaf
Haidomyrmex sp4	0.0192	0.1936	0.02	0.0242	0.0262	0.2316	0.3518	0.055	0.0784	0	pred_leaf
Haidomyrmex indet1	0.0156	0.1758	0.0162	0.0238	0.0206	0.267	0.3672	0.0548	0.058	0.001	pred_leaf
Haidomyrmex indet2	0.0134	0.1458	0.0116	0.1266	0.0158	0.119	0.3458	0.1424	0.0794	2.00E-04	pred_leaf

Table S47.

Ecomorph prediction votes when using model trained on subset of complete morphometrics dataset, log-shape variable measurements; functional morphology.

Species	Cn	Gr	Lg	Ll	Sb	Predicted aspect
Ceratomyrmex planus	0.0826	0.3726	0.049	0.4512	0.0446	Ll
Ceratomyrmex ellenbergeri	0.0784	0.4816	0.0228	0.3806	0.0366	Gr
Ceratomyrmex ellenbergeri	0.0618	0.3738	0.0342	0.488	0.0422	Ll
Ceratomyrmex ellenbergeri	0.0442	0.4592	0.0816	0.3652	0.0498	Gr
Protoceratomyrmex revelatus	0.058	0.4034	0.0646	0.4356	0.0384	Ll
Linguamyrmex sp5	0.0356	0.4168	0.0062	0.5208	0.0206	Ll
Linguamyrmex sp4	0.0402	0.378	0.017	0.538	0.0268	Ll
Linguamyrmex brevicornis	0.1576	0.1788	0.094	0.546	0.0236	Ll
Linguamyrmex sp2	0.07	0.3254	0.0278	0.5388	0.038	Ll
Linguamyrmex sp1	0.0532	0.4182	0.0364	0.4416	0.0506	Ll
Haidomyrmex sp3	0.0136	0.1222	0.4748	0.3456	0.0438	Lg
Haidomyrmex sp5	0.0236	0.408	0.08	0.4736	0.0148	Ll
Haidomyrmex sp5	0.0402	0.3582	0.0678	0.5082	0.0256	Ll
Haidomyrmex sp5	0.0212	0.3798	0.1676	0.396	0.0354	Ll
Haidomyrmex sp5	0.037	0.1992	0.317	0.3978	0.049	Ll
Haidomyrmex scimitarus	0.0628	0.375	0.045	0.4716	0.0456	Ll
Haidomyrmex sp5	0.0142	0.3124	0.2436	0.365	0.0648	Ll
Haidomyrmex sp4	0.0262	0.3586	0.142	0.4406	0.0326	Ll

Haidomyrmex indet1	0.0268	0.3394	0.13	0.4684	0.0354	Ll
Haidomyrmex indet2	0.0186	0.3626	0.162	0.4262	0.0306	Ll

Table S48.

Nesting niche prediction votes when using model trained on subset of complete morphometrics dataset, log-shape variable measurements; homologous morphology.

Species	Ab	CR	Eg	Ll	Predicted aspect
Ceratomyrmex planus	0.1662	0.0568	0.2846	0.4924	Ll
Ceratomyrmex ellenbergeri	0.1582	0.031	0.3118	0.499	Ll
Ceratomyrmex ellenbergeri	0.1248	0.0416	0.3102	0.5234	Ll
Ceratomyrmex ellenbergeri	0.1452	0.1064	0.29	0.4584	Ll
Protoceratomyrmex revelatus	0.135	0.069	0.3774	0.4186	Ll
Linguamyrmex sp5	0.0552	0.0238	0.317	0.604	Ll
Linguamyrmex sp4	0.0862	0.0284	0.3164	0.569	Ll
Linguamyrmex brevicornis	0.2326	0.0652	0.1356	0.5666	Ll
Linguamyrmex sp2	0.1406	0.0558	0.2954	0.5082	Ll
Linguamyrmex sp1	0.1288	0.0486	0.3258	0.4968	Ll
Haidomyrmex sp3	0.3742	0.218	0.1058	0.302	Ab
Haidomyrmex sp5	0.1432	0.086	0.297	0.4738	Ll
Haidomyrmex sp5	0.1374	0.0982	0.3052	0.4592	Ll
Haidomyrmex sp5	0.1838	0.125	0.2616	0.4296	Ll
Haidomyrmex sp5	0.294	0.199	0.1668	0.3402	Ll
Haidomyrmex scimitarus	0.1294	0.0678	0.326	0.4768	Ll
Haidomyrmex sp5	0.207	0.118	0.2002	0.4748	Ll
Haidomyrmex sp4	0.155	0.1198	0.2902	0.435	Ll

Haidomyrmex indet1	0.1522	0.1192	0.2776	0.451	Ll
Haidomyrmex indet2	0.1544	0.1236	0.2832	0.4388	Ll

Table S49.

Foraging niche prediction votes when using model trained on subset of complete morphometrics dataset, log-shape variable measurements; homologous morphology.

Species	Fg	Gn	GP	Om	Py	SP	Predicted aspect
Ceratomyrmex planus	0.0526	0.1876	0.1334	0.2536	0.0062	0.3666	SP
Ceratomyrmex ellenbergeri	0.0434	0.0884	0.237	0.4156	0.0074	0.2082	Om
Ceratomyrmex ellenbergeri	0.0424	0.0982	0.2884	0.3152	0.0014	0.2544	Om
Ceratomyrmex ellenbergeri	0.033	0.1188	0.2166	0.317	0.009	0.3056	Om
Protoceratomyrmex revelatus	0.022	0.0202	0.1314	0.3288	0.0114	0.4862	SP
Linguamyrmex sp5	0.0532	0.1232	0.247	0.387	0.007	0.1826	Om
Linguamyrmex sp4	0.0408	0.0478	0.2056	0.3484	0.0066	0.3508	SP
Linguamyrmex brevicornis	0.032	0.049	0.1414	0.2564	0.0112	0.51	SP
Linguamyrmex sp2	0.0582	0.0512	0.2278	0.324	0.0072	0.3316	SP
Linguamyrmex sp1	0.0362	0.0588	0.2594	0.405	0.0076	0.233	Om
Haidomyrmex sp3	0.0036	0.0042	0.324	0.1058	0.101	0.4614	SP
Haidomyrmex sp5	0.003	0.0082	0.3546	0.2944	0.0206	0.3192	GP
Haidomyrmex sp5	0.0056	0.0062	0.4012	0.2294	0.0212	0.3364	GP
Haidomyrmex sp5	0.0026	0.0298	0.2894	0.219	0.0462	0.413	SP
Haidomyrmex sp5	0.0186	0.0334	0.3224	0.1716	0.0522	0.4018	SP
Haidomyrmex scimitarus	0.0236	0.0414	0.32	0.313	0.0082	0.2938	GP
Haidomyrmex sp5	0.0016	0.016	0.2758	0.1076	0.0928	0.5062	SP
Haidomyrmex sp4	0.0052	0.0418	0.3006	0.164	0.0578	0.4306	SP

Haidomyrmex indet1	0.0016	0.013	0.3696	0.2216	0.03	0.3642	GP
Haidomyrmex indet2	0.0036	0.0402	0.255	0.1484	0.0568	0.496	SP

Table S50.

Functional role prediction votes when using model trained on subset of complete morphometrics dataset, log-shape variable measurements; homologous morphology.

Species	om_cn_ab	om_grll_eg	om_leaf	om_lg_ab	pred_cr	pred_gr_egll	pred_leaf	pred_lg_ab	pred_ll_eg	pred_sub	Predicted aspect
Ceratomyrmex planus	0.062	0.2386	0.1822	0.0032	0.0194	0.1806	0.2468	0.0564	0.0058	0.005	pred_leaf
Ceratomyrmex ellenbergeri	0.0832	0.3168	0.1506	0.0024	0.0182	0.159	0.2412	0.0138	0.013	0.0018	om_grll_eg
Ceratomyrmex ellenbergeri	0.075	0.256	0.1694	0.0016	0.0258	0.1868	0.2578	0.0156	0.0102	0.0018	pred_leaf
Ceratomyrmex ellenbergeri	0.0556	0.2986	0.112	0.0048	0.0382	0.1558	0.2606	0.0502	0.0188	0.0054	om_grll_eg
Protoceratomyrmex revelatus	0.052	0.3228	0.0306	0.005	0.0204	0.1462	0.2766	0.0724	0.0696	0.0044	om_grll_eg
Linguamyrmex sp5	0.0506	0.2688	0.1762	4.00E-04	0.0052	0.1628	0.324	0.0078	0.0026	0.0016	pred_leaf
Linguamyrmex sp4	0.0538	0.2644	0.1282	0.001	0.0086	0.1702	0.3502	0.0148	0.0072	0.0016	pred_leaf
Linguamyrmex brevicornis	0.1362	0.13	0.05	0.0046	0.0198	0.066	0.469	0.0882	0.033	0.0032	pred_leaf
Linguamyrmex sp2	0.0838	0.2446	0.1132	0.0014	0.0278	0.154	0.3418	0.0254	0.0058	0.0022	pred_leaf
Linguamyrmex sp1	0.0702	0.2666	0.1188	0.0016	0.0272	0.1674	0.3092	0.0194	0.0174	0.0022	pred_leaf
Haidomyrmex sp3	0.0118	0.0388	0.0028	0.1434	0.0334	0.0326	0.2692	0.4268	0.028	0.0132	pred_lg_ab

Haidomyrmex sp5	0.0244	0.2566	0.014	0.0154	0.0138	0.108	0.485	0.0508	0.0304	0.0016	pred_leaf
Haidomyrmex sp5	0.03	0.247	0.013	0.011	0.0186	0.1454	0.4418	0.0518	0.0362	0.0052	pred_leaf
Haidomyrmex sp5	0.0214	0.2156	0.0086	0.0574	0.0254	0.1154	0.3776	0.111	0.0582	0.0094	pred_leaf
Haidomyrmex sp5	0.0432	0.1142	0.0362	0.1226	0.0578	0.0582	0.2544	0.2642	0.0384	0.0108	pred_lg_ab
Haidomyrmex scimitarus	0.0598	0.2394	0.0922	0.0032	0.0228	0.2304	0.3066	0.027	0.0156	0.003	pred_leaf
Haidomyrmex sp5	0.0064	0.095	0.0074	0.2178	0.0136	0.1068	0.2562	0.1764	0.0956	0.0248	pred_leaf
Haidomyrmex sp4	0.0276	0.2278	0.0128	0.0218	0.035	0.1298	0.4024	0.0826	0.0536	0.0066	pred_leaf
Haidomyrmex indet1	0.023	0.2272	0.011	0.026	0.0318	0.127	0.4248	0.0804	0.0408	0.008	pred_leaf
Haidomyrmex indet2	0.0148	0.1566	0.011	0.1254	0.0274	0.1138	0.3098	0.1684	0.0654	0.0074	pred_leaf

Table S51.

Ecomorph prediction votes when using model trained on subset of complete morphometrics dataset, log-shape variable measurements; homologous morphology.

Lineage	Average ecological disparity	Standard deviation of ecological disparity
Ponerines (*Anochetus* and *Odontomachus*)	4.701	2.553
Dacetines (*Acanthognathus*, *Daceton*, *Epopostruma*, *Microdaceton*, and *Orectognathus*)	4.667	2.570
Strumigenys	3.200	1.600
Myrmoteras	1.333	0.471
Haidomyrmecines (conservative estimate)	2.944	1.632
Haidomyrmecines (comprehensive estimate)	3.448	1.746

Table S52.
Average and standard deviation of ecological disparity calculated as pairwise distances between each unique three-dimensional occupation. Haidomyrmecine conservative estimates are derived from only the majority aspect predicted by the raw functional measurement model, while comprehensive estimates are derived from majority aspects predicted from all four RF models.